Nucleic Acids Research, 2024, **52**, 8643–8660
https://doi.org/10.1093/nar/gkae558
Advance access publication date: 28 June 2024
NAR Breakthrough Article

NAR Breakthrough Article

PCAF promotes R-loop resolution via histone acetylation

Seo Yun Lee [1,*], Soo Hyeon Lee [1], Nak Hun Choi [1], Ja Young Kim [1], Jun Hee Kweon [1], Kyle M. Miller [2] and Jae Jin Kim [1,*]

[1]Department of Life Science and Multidisciplinary Genome Institute, Hallym University, Chuncheon 24252, Republic of Korea
[2]Department of Molecular Biosciences, The University of Texas at Austin, Austin, TX 78712, USA

[*]To whom correspondence should be addressed. Tel: +82 033 248 2094; Fax: +82 033 256 3420; Email: jjkim@hallym.ac.kr
Correspondence may also be addressed to Seo Yun Lee. Tel: +82 033 248 2094; Fax: +82 033 256 3420; Email: seoyun@hallym.ac.kr

Abstract

R-loops cause genome instability, disrupting normal cellular functions. Histone acetylation, particularly by p300/CBP-associated factor (PCAF), is essential for maintaining genome stability and regulating cellular processes. Understanding how R-loop formation and resolution are regulated is important because dysregulation of these processes can lead to multiple diseases, including cancer. This study explores the role of PCAF in maintaining genome stability, specifically for R-loop resolution. We found that PCAF depletion promotes the generation of R-loop structures, especially during ongoing transcription, thereby compromising genome stability. Mechanistically, we found that PCAF facilitates histone H4K8 acetylation, leading to recruitment of the a double-strand break repair protein (MRE11) and exonuclease 1 (EXO1) to R-loop sites. These in turn recruit Fanconi anemia (FA) proteins, including FANCM and BLM, to resolve the R-loop structure. Our findings suggest that PCAF, histone acetylation, and FA proteins collaborate to resolve R-loops and ensure genome stability. This study therefore provides novel mechanistic insights into the dynamics of R-loops as well as the role of PCAF in preserving genome stability. These results may help develop therapeutic strategies to target diseases associated with genome instability.

Graphical abstract

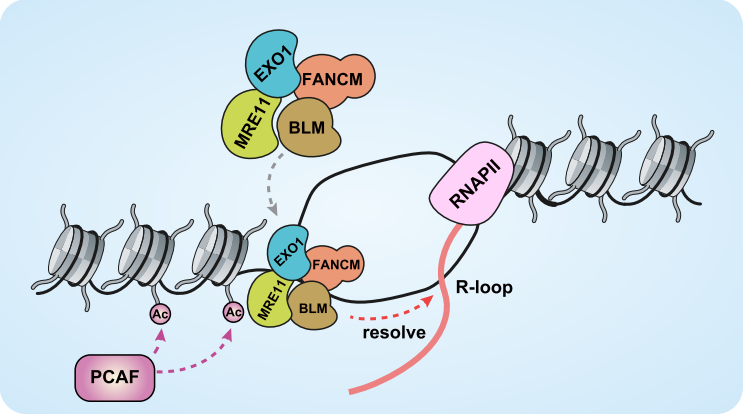

Introduction

R-loops are nucleic acid structures composed of three strands, which arise when RNA hybridizes with a DNA template strand during transcription (1,2). The RNA and DNA form a stable hybrid, causing the exposure of the non-template DNA strand. While R-loops are essential for many cellular processes, including transcription, replication, and DNA repair, their prolonged existence and accumulation can induce genomic instability, potentially contributing to diseases, such as cancer (3–5). Due to these health implications, understanding the mechanisms governing R-loop formation and resolution is vital.

To ensure genome integrity during transcription, cells employ several enzymes to resolve R-loops and preserve the DNA (4). Endoribonucleases, such as RNase H1 and RNase H2, can cleave off the RNA in RNA/DNA hybrids (6,7); RNA splicing factors, including serine and arginine-rich splicing factor 1 (SRSF1) and splicing factor 3B subunit 1 (SF3B1) prevent R-loop formation (8,9); topoisomerases remove R-loops to prevent replication stress (10–12); and RNA/DNA helicases, such as Senataxin (SETX), FA complementation group M (FANCM), and BLM RecQ like helicase (BLM) unwind RNA/DNA hybrids (11,13–15). In addition, the MRE11–RAD50–NBS1 (MRN) complex suppresses R-loop forma-

Received: March 5, 2024. **Revised:** June 4, 2024. **Editorial Decision:** June 12, 2024. **Accepted:** June 19, 2024

tion independently of its catalytic activity (16) and maintains genome stability by leveraging the nuclease activity of MRE11. Moreover, it also serves a structural function by acting as a DNA tether and platform for DNA damage signaling (17). During R-loop resolution, MRN can collaborate with other helicases, where it uses its structural capability to recruit RNA/DNA helicases such as FANCM and BLM to the R-loop accumulation sites (16).

Exonuclease 1 (EXO1) is important for signaling DNA damage mediated by RNA/DNA hybrids (18). These hybrids act as platforms for DNA repair proteins at sites of double-strand breaks (DSBs). For example, BRCA1 recognizes RNA/DNA hybrids near DSBs at DNA damage sites and recruits RNase H2 and EXO1. Next, EXO1 resects the DNA strand, while RNase H2 degrades the RNA. This facilitates the formation of RAD51 nucleofilaments and ensures proper homologous recombination (HR) repair (19). However, the function of EXO1 in resolving R-loops at transcription sites and the mechanisms by which MRN and EXO1 are recruited to the R-loop accumulation sites remain unclear. In a previous study, we found that MRE11 and EXO1 were recruited at the replication fork during histone acetylation (20). Furthermore, histone acetylation is critical for nuclease recruitment (20).

PCAF (p300/CBP-associated factor) is a histone acetyltransferase (HAT) that regulates gene expression. It belongs to the GNAT (Gcn5-related N-acetyltransferase) superfamily of HAT enzymes and is highly conserved in eukaryotes. PCAF can acetylate lysine residues of histones present in the chromatin structure of DNA; this acetylation alters chromatin structure and allows for the activation or repression of gene expression (21). In addition to its role in transcriptional regulation, PCAF is also involved in various cellular processes, including DNA repair, cell cycle progression, and apoptosis (11,20,22,23). Furthermore, dysregulation of PCAF has been implicated in cancers (20,24,25). Understanding the mechanisms regulating PCAF activity may facilitate the development of new therapeutic strategies for cancer treatment. To that end, we observed a decrease in PCAF expression in various cancers, which prompted us to assess its role in transcription-mediated endogenous DNA damage.

Here, we report that PCAF-mediated histone acetylation is a crucial signaling event that facilitates the recruitment of R-loop-resolving enzymes. Specifically, PCAF promotes the resolution of accumulated R-loops by acetylating histone H4 at lysine 8 (H4K8ac), thereby enhancing recruitment of MRE11 and EXO1 to the R-loop site. In addition, we found that PCAF-mediated histone acetylation can eliminate pathological R-loops in cells that are depleted of BRCA and SETX. Overall, our findings highlight that PCAF and histone acetylation are essential components for safeguarding against endogenous DNA damage during transcription.

Materials and methods

Cell lines and culture

U2OS and HEK-293 cells were purchased from ATCC (HTB-96 and CRL-1573, respectively) and cultured in Dulbecco's modified Eagle's medium (DMEM) supplemented with 10% FBS and 1% penicillin/streptomycin. RPE and MRC5 cells were kindly provided from Dr Kyle M. Miller (The University of Texas at Austin, TX). These cells were cultured in DMEM supplemented with 10% FBS and 1% penicillin/streptomycin. U2OS-PCAF knockout (KO) cell lines were generated using the CRISPR/Cas9 system, as previously described (11). U2OS-MRE11 or -EXO1 knockdown (KD) cell lines were made with shMRE11 (Sigma-Aldrich, #TRCN0000039868) and shEXO1 (Sigma-Aldrich, # TRCN0000039788) lentiviral constructs. RPE- and MRC5-PCAF knockdown (KD) cell lines were made with shPCAF (Sigma-Aldrich, TRCN0000018528) lentiviral constructs. Lentiviral vectors (pLKO.1-shRNAs) were obtained from Sigma-Aldrich and transfected into HEK-293 cells with an envelope vector (pMD2.G), and packing vectors (pRSV-Rev and pMDLg/RRE) using Lipofectamine 2000 (Invitrogen). Transfected cells were changed to fresh medium the following day, and the lentivirus-containing medium was harvested 48 h, 72 h post-transfection. U2OS cells were infected with the virus-containing medium in the presence of polybrene (8.3 μg/ml) and selected with puromycin (2 μg/ml) for 3 days. The knockdown (KD) cells were validated by western blotting using specific antibodies. For siRNA-based knockdown cells, U2OS cells were transfected with siRNA using Lipofectamine RNAiMAX or Lipofectamine 2000 and then, knockdown efficiency was confirmed by western blotting and qRT-PCR. The qRT-PCR primers are listed in Supplementary Table S1 and the siRNA sequences used in this study are as follows:

Control siRNA (siCtrl) : 5′-AACGUACGCGGAAUACUU CGAUU-3′
MRE11 siRNA : 5′-ACAGGAGAAGAGAUCAACUUU-3′
EXO1 siRNA : 5′-GGAUGUACUUUACCUUCUAUU-3′
CtIP siRNA : 5′-GCUAAAACAGGAACGAAUCUU-3′
SETX siRNA : 5′-GAGAGAAUUAUUGCGUACUUU-3′
FANCD2 siRNA : 5′-CCUUAGAUGUCCUUCUAGAUU-3′

Plasmids and cloning

PCAF, MRE11 and EXO1 were cloned into the pENTR/D-TOPO vector (Invitrogen) and entry clones were then transferred into various destination vectors (pcDNA6.2 N-EmGFP, pDEST-CMV-SFB and pDEST20) using the Gateway LR Cloning system (Invitrogen). The deletion mutants were generated by Q5 Site-direct mutagenesis (NEB), and point mutants were constructed using QuikChange Site-directed mutagenesis (Agilent Technologies), following the manufacturer's instructions. All primer sequences are summarized in Supplementary Table S1.

Antibodies

Primary antibodies used in this study were Anti-S9.6 (Kerafest, #ENH001); Anti-ssDNA (Millipore, #MAB3034); Anti-Nucleolin (Abcam, #ab50279); Anti-PCAF (Cell Signaling, #3378); Anti-H4K8ac (Millipore, #07-328); Anti-MRE11 (Novus Biologicals, #NB100-142); Anti-EXO1 (Genetex, #GTX109891); Anti-FANCM (Cell Signaling, #57697); Anti-BLM (Abcam, #ab2179); Anti-GFP (Abcam, #ab290); Anti-mCherry (Abcam, #ab167453); Anti-Flag (Sigma-Aldrich, #F1804; Millipore, #F7425), Anti-β-actin (Sigma-Aldrich, #A5441); Anti-mouse IgG isotype control (Santa-Cruz, #sc-2025). Secondary antibodies used were anti-mouse HRP (Cell Signaling, #7076), anti-rabbit HRP (Cell Signaling, #7074), Alexa Fluor 488 goat anti-mouse IgG (Invitrogen, #A11029), Alexa Fluor 594 goat anti-mouse IgG (Invitrogen,

#A11032), Alexa Fluor 488 goat anti-rabbit IgG (Invitrogen, #A11034), Alexa Fluor 594 goat anti-rabbit IgG (Invitrogen, #A11037).

Western blotting

Samples were subjected to electrophoresis on an 8–16% gradient SDS-PAGE gel for 90 min (120 V) and were subsequently transferred onto a nitrocellulose membrane (Cytiva) for 2 h at 100V. The transferred membranes were blocked with 3% BSA in TBS-T (0.05% Tween-20) for 1 h and incubated with the specific primary antibody at 4°C overnight with gentle shaking. Membranes were washed 3 times with TBS-T and then incubated with the appropriate secondary antibody for 1 h at room temperature, with gentle shaking. Following another 3 times washing, the membranes were visualized using ECL (GE Healthcare) and imaged with a ChemiDoc instrument (Bio-Rad) through chemiluminescence.

Single-cell gel electrophoresis (neutral comet assay)

The neutral comet assay was conducted to measure DNA double-strand breaks (DSBs) using the CometAssay Reagent kit (Trevigen), following the manufacturer's instructions. Briefly, cells were harvested with trypsin-EDTA and washed once with PBS. Cell pellets were mixed with LMAgarose and applied to glass slides. The cells were lysed with comet lysis buffer at 4°C for 1 h, and slides were subjected to electrophoresis (1 V/cm^2) for 40 min in TBE buffer using a submerged horizontal electrophoresis system (Bio-Rad). Subsequently, samples were fixed with 70% EtOH for 10 min, and dried at room temperature. The dried slides were stained with SYBR-green (Invitrogen) for 10 min and the comet images were captured using a fluorescence microscope (Eclipse Ti2, Nikon). Comet tail moments were calculated using ImageJ and graphed using Prism software. The tail moment (TM) reflects both the tail length (TL) and the fraction of DNA in the comet tail (TM = %DNA in tail × TL/100).

Immunofluorescence for R-loop

Cells were fixed with 100% ice-cold methanol at 4°C for 20 min and 3 times washed with PBS at room temperature. Cells were then blocked with 3% BSA/PBST for 1 h and incubated with the S9.6 antibody (Kerafast) at 4°C for 18 h. The co-stained samples were used with appropriate antibodies and cells were washed with PBS after primary antibody incubation. Cells were then incubated with Alexa Fluor secondary antibody in 3% BSA/PBST for 1 h and mounted with Vectashield mounting medium containing DAPI (Vector Labs). Images were captured using a fluorescence microscope (Eclipse Ti2, Nikon) or Fluoview FV 3000 confocal microscope (Olympus) and nucleoplasmic S9.6 signals were quantified using ImageJ.

GFP-dRH protein purification and immunofluorescence

The purification of GFP-dRH was performed as described in (26,27). Briefly, an N-terminal tandem His-GFP-tagged RNase H1 D210 (GFP-dRH) plasmid was purchased from Addgene (#174448), and transformed into *E. coli* BL21 (DE3). Cells were cultured in LB broth until the OD_{600} reached 0.5 and then induced with IPTG (final concentration of 0.4 mM). The cell pellet was lysed with lysis buffer (50 mM Tris–Cl, pH 7.5, 50 mM NaCl, 5 mM EDTA, 1 mM EGTA, 1 mM DTT, 0.2% Triton X-100, 100 ng/μl lysozyme, and 1 mM PMSF) and sonicated 3 times (10 s pulse ON/OFF). The soluble fraction was collected by centrifugation, and the supernatants were used to purify the His-GFP-dRH with a MagListo™ His-tagged protein purification kit (Bioneer). To image the R-loop with GFP-dRH, cells were fixed with 100% ice-cold methanol at –20°C for 5 min and washed 3 times with PBS at room temperature. Cells were then permeabilized with 0.25% Triton X-100 for 10 min and pretreated with RNase H (NEB, M0297) for enzymatic digestion. Samples were blocked with 3% BSA (in PBS) for 30 min and incubated with a 1:2000 dilution of GFP-dRNH1 (0.2 mg/ml) in 3% BSA for 2 h at 37°C. After incubation, samples were washed 3 times with TBST and mounted with a Vectashield mounting medium containing DAPI (Vector Labs). Images were captured using a fluorescence microscope (Eclipse Ti2, Nikon) and signals were quantified using ImageJ.

Dot blot assay for R-loop

The dot blot assay for R-loop detection was performed as previously described (11). To assess the R-loop level, total genomic DNA was isolated from cells using the DNeasy Blood and Tissue kit (Qiagen). The isolated genomic DNA was spotted as a dot on a nitrocellulose membrane and UV-crosslinked. The membrane was detected using S9.6 and ssDNA antibodies in 1% BSA/TBST, and images were acquired with ChemiDoc (Bio-Rad). The intensity was calculated by ImageJ and S9.6 intensity was normalized to the ssDNA signal. RNase H (NEB, M0297) treated sample was used as a negative control for R-loop.

R-loop Immunoprecipitation (R-loop IP)

R-loop IP was performed as previously described (28,29). Briefly, cells were harvested and lysed with lysis buffer (85 mM KCl, 5 mM PIPES, pH 8.0, and 0.5% NP-40, protease inhibitor cocktail) for 10 min on ice. Subsequently, cells were centrifuged at 500 × g at 4°C for 5 min, and pelleted nuclei were resuspended in nuclear lysis buffer (10 mM Tris–HCl, pH 7.5, 200 mM NaCl, 2.5 mM $MgCl_2$, 0.2% sodium deoxycholate, 0.1% SDS, 0.05% sodium lauroyl sarcosinate). The lysate was sonicated 4 times (10 s pulse ON/OFF) and diluted in S9.6 IP buffer (10 mM Tris–HCl, pH 7.5, 200 mM NaCl, 2.5 mM $MgCl_2$, 0.05% sodium deoxycholate, 0.025% SDS, 0.0125% sodium lauroyl sarcosinate) with protease inhibitor cocktail. R-loops were immunoprecipitated at 4°C for 2 h with BSA-blocked protein A/G beads conjugated to the S9.6 antibody. After incubation, the samples were treated with RNase A and washed with RSB (10 mM Tris–HCl, pH 7.5, 200 mM NaCl, 2.5 mM $MgCl_2$) and RSB with 0.5% Triton X-100 buffer. The bead-bound proteins were eluted with SDS sample buffer and boiled supernatants were separated by 8–16% SDS-PAGE.

Proximity ligation assay

A proximity ligation assay was performed using the Duolink *In Situ* PLA kit (Sigma-Aldrich), following the manufacturer's instructions with a few modifications accordingly to reference (30,31). In brief, cells were washed with ice-cold PBS and pre-extracted with CSK buffer (10 mM PIPES, pH 6.8, 100 mM NaCl, 300 mM sucrose, 3 mM $MgCl_2$, 1 mM EGTA, 0.5%

Triton X-100) for 10 min on ice and then, cells were fixed with 4% paraformaldehyde (PFA) for 15 min. In case of PLA with S9.6 antibody, cells were treated with RNase solution (0.1% BSA, 3 mM $MgCl_2$, 1:200 RNase T1, 1:200 shortcut RNase III in PBS) for 1 h at room temperature. Subsequently, cells were washed with PBS and blocked with the Duolink blocking solution at 37°C for 1 h. Primary antibodies were diluted in the Duolink antibody dilutant and incubated at 4°C for overnight. On the following day, cells were washed with PBS and incubated with the diluted PLA probe (anti-mouse and anti-rabbit) at 37°C for 1 h. Cells were then washed twice with pre-warmed PLA washing buffer A and incubated with the ligation mix for 30 min. Finally, cells were incubated with the amplification mix for 100 min at 37°C and washed with pre-warmed PLA washing buffer B. Cells were mounted with DAPI-containing Vectashield mounting medium (Vector lab) and detected using a fluorescence microscope (Eclipse Ti2, Nikon). PLA intensity was quantified using ImageJ and analyzed by Prism software.

mRNA quantification

The RNA was extracted using the RNeasy Kit (Qiagen) following the manufacturer's recommendations. The isolated total RNA was reverse-transcribed into cDNA using the High-Capacity cDNA Reverse Transcription kit (Applied Biosystems). Various mRNA abundances were quantified using quantitative reverse transcription-polymerase chain reaction (qRT-PCR) with specific targeting primers. Detailed information for qPCR primer sequences is described in Supplementary Table S1.

DNA-RNA hybrid immunoprecipitation (DRIP) assay

The DNA-RNA hybrid immunoprecipitation (DRIP) assay was performed as described in (32) using the S9.6 antibody. Briefly, cells were harvested using trypsin-EDTA and resuspended in TE buffer. Subsequently, cells were lysed with 50 μl of 20% SDS and 5 μl of protease K (20 mg/ml) at 37°C overnight. On the following day, the lysates were precipitated with phenol/chloroform/isoamyl alcohol (25:24:1) and purified genomic DNA (gDNA) was digested with a cocktail of restriction enzymes at 37°C overnight. After enzyme digestion, gDNA precipitated using phenol/chloroform/isoamyl alcohol and ethanol method. For the negative control, the digested gDNA was incubated with RNase H enzyme (NEB) at 37°C for 3 h and precipitated using phenol/chloroform/isoamyl alcohol and ethanol. The appropriate amount of digested gDNA was incubated with S9.6 antibody at 4°C overnight and incubated with protein A/G beads at 4°C for 2 h. The samples were analyzed by qPCR using a specific primer, and primer sequences are detailed in Supplementary Table S1.

Chromatin immunoprecipitation (ChIP) assay

The ChIP assay was performed using SimpleChIP® Enzymatic Chromatin IP Kit (Cell Signaling) according to the manufacturer's protocol. Briefly, cells were crosslinked for 10 min with 1% PFA and then quenched with glycine. Subsequently, cells were lysed in ChIP lysis buffers A and B and subjected to sonication. The samples were centrifuged, and the supernatants were incubated with the primary antibody at 4°C for 18 h. The antibody-bound proteins/DNA were then pulled down with protein A/G beads and eluted with a ChIP elution buffer. Eluted protein/DNA was digested with protease K, and the resulting purified DNA was analyzed by quantitative PCR (qPCR) for both input and ChIPed DNAs. Detailed primer sequences are provided in Supplementary Table S1.

5-EU incorporation assay

The global RNA transcription was measured using the Click-it RNA Imaging kit (Invitrogen). The newly synthesized RNA was labeled with 5-ethynyl uridine (5-EU) for 10 min and rinsed in cold medium and PBS before fixation in 2% paraformaldehyde (PFA). 5-EU incorporation was stained following the manufacturer's instructions and visualized using a fluorescence microscope (Eclipse Ti2, Nikon). Intensity was calculated using ImageJ.

Recombinant protein purification from Sf9 cell

The Sf9 cells were cultured in SF-900 III SFM medium (Invitrogen) at 28°C and transfected with EXO1-bacmid DNA using Cellfectin II reagent (Invitrogen). After 5 days, the baculovirus-containing supernatant was harvested and infected into new Sf9 cells. For protein purification, cells were collected and lysed with NETN lysis buffer (25 mM Tris–HCl, pH 8.0, 150 mM NaCl, 1 mM EDTA, 1 mM DTT, 1% NP-40, 0.1% Triton X-100, protease inhibitor cocktail, and 1 mM PMSF). The lysate was sonicated 3 times (10s pulse ON/OFF), and soluble protein extracts were incubated with Glutathione-Sepharose 4B resins. GST-resins were washed with NETN buffer, and bound proteins were eluted by elution buffer containing reduced glutathione (50 mM HEPES, pH 7.5, 100 mM NaCl, 30% glycerol, 0.03% Triton X-100, 40 mM reduced glutathione). The purified proteins were analyzed by SDS-PAGE and visualized by Coomassie brilliant blue staining (Bio-Rad). MRE11 proteins were purified, as referred (33). pDEST20-MRE11 and pACEBac1-Rad50 were transformed into DH10Bac *E. coli* and transfected into Sf9 cells using Cellfectin II reagent (Invitrogen), respectively. Each baculovirus was amplified through 2–3 rounds by the usual method. Upon isolation of MRE11 proteins, MRE11-expresing baculovirus was infected into Sf9 cell along with Rad50-expressing baculovirus and subjected to pulldown using Glutathione-Sepharose 4B resins.

In vitro R-loop cleavage assay

For the R-loop cleavage assay, substrate oligonucleotides were synthesized as described with minor modification (34). Briefly, non-labeled DNA oligonucleotides were combined with 5′-Cy3-labeled RNA or DNA at a molar ratio of 1.5:1 with annealing buffer (20 mM Tris–HCl, pH 7.5, 10 mM $MgCl_2$, 2 mM DTT and 50 mM KCl). Then the 100 nM oligonucleotide mixtures were heated at 95°C for 2 min and allowed to cool down to room temperature overnight. The synthesized substrates (50 fmol) were incubated with recombinant MRE11 or EXO1 proteins in NEB buffer 4 at 4°C. The reactions were terminated by stop buffer (2% SDS, 20% glycerol, 0.1 mM EDTA, 5 mg/ml proteinase K, and 0.05% bromophenol blue, xylene cyanol) and further incubated for 10 min at 37°C. Samples were separated using an 18% native PAGE and were subsequently detected with Cy3 using a ChemiDoc (Bio-Rad). Image quantification was performed with ImageJ and normalized against the control. The sequences of these oligonucleotide substrates are as follows:

A : 5′-(Cy3) AGCTATGACCATGATTACGAATTGC-3′
B : 5′-(Cy3) AGCUAUGACCAUGAUUACGAAUUGC-3′
C : 5′-GCAATTCGTAATCATGGTCATAGCTTTTTTTTT TTTTTTTTTTTTT-3′
D : 5′-GGGTGAACCTGCAGGTGGGCTTTTTTTTTT TTTTTTTTTTTTTTTTGGTAGAATTCG GCAGCGTC-3′
E: 5′-GACGCTGCCGAATTCTACCAGCAATTCGTAAT CATGGTCATAGCTGCCCACCTGCA GGTTCACCC-3′

Analysis of data from publicly available databases

Fraction of Genome Altered data from The Cancer Genome Atlas (TCGA) were analysis from cBioportal. The GSE13911 dataset was acquired from Gene Expression Omnibus (GEO) and the expression analysis were using GEO2R tool. KAT2B expression data from TCGA were acquired from UALCAN cancer data analysis portal (https://ualcan.path.uab.edu).

Quantification and statistical analysis

The intensity for dot blot assay and fluorescence image were measured by ImageJ. Graphs were generated and statistical analyses were performed using Prism software. One-way analysis of variance (ANOVA) was used when comparing more than two groups, followed by the Dunnett multiple comparison test. Comparisons between the two groups were made with the student's *t*-test or Mann–Whitney test as indicated. Figure legends include *P*-values, sample size, and experiments were repeated at least 3 times using biologically independent.

Results

PCAF expression is downregulated in various human cancers

Previous studies have shown that the dynamics of histone acetylation are closely linked to important cellular functions, including DNA replication, DNA repair, and RNA transcription (35–37). Likewise, the histone acetyltransferase PCAF plays a significant role in regulating oncogenes and tumor suppressors by acetylating histones and transcription factors, which ultimately affect cancer progression (38–40). To investigate the potential importance of PCAF, we first analyzed the expression pattern of *KAT2B* (PCAF) in the Cancer Genome Atlas samples using the UALCAN (https://ualcan.path.uab.edu/index.html) database. Pan-cancer analysis indicated that among the 24 cancers, *KAT2B* expression was significantly downregulated in most cancers (Figure 1A). Using the cBioPortal platform, we found that *KAT2B* (PCAF) expression was accompanied by genome alterations in multiple cancers, including gastric, breast, colon, and ovarian cancer (Figure 1B). The fraction of genome altered represents the percentage of the genome affected by copy number gains or losses due to genome instability. These results suggest that reduced *KAT2B* (PCAF) levels may be involved in the genomic integrity of various human cancers.

PCAF depletion triggers endogenous DNA damage

To investigate the role PCAF plays regarding genome integrity, we generated PCAF knockout (KO) U2OS cells (Supplementary Figure S1A). PCAF can act as a coactivator of several transcriptional activators that are involved in cell growth and development (21). Therefore, we investigated the role of PCAF in transcription using the 5-ethynyl uridine (5-EU) incorporation method (Figure 1C). Consistent with previous findings, we observed that 5-EU incorporation was significantly reduced in PCAF KO cells, indicating that loss of PCAF was correlated with disturbance of transcription. We hypothesized that disrupted transcription processes in PCAF-deficient cells might lead to intrinsic DNA damage even in the absence of external DNA-damaging agents. To test this hypothesis, we assessed DNA damage levels after treatment with the transcription inhibitor triptolide, which is known to induce collapse of the transcription bubble and degrade RNA polymerase II (41). Transcription inhibition by triptolide treatment was confirmed by 5-EU incorporation through quantification of *de novo* RNA synthesis (Supplementary Figure S1B). As expected, increased DNA breaks in PCAF KO cells were remarkably suppressed by transcriptional inhibition (Figure 1D). Taken together, these data indicate that DNA damage that occurs due to PCAF depletion requires the presence of active transcription bubbles.

PCAF depletion induces R-loop accumulation

During transcription, RNA polymerase binds to template DNA and synthesizes an RNA strand. Occasionally, the nascent RNA product can hybridize with the template DNA strand, forming an R-loop composed of an RNA/DNA hybrid and displaced non-templated DNA (2,42,43). Since the accumulation of aberrant R-loops during transcription has been shown to cause DNA breakage (44–46), we postulated that this might be the underlying cause of DNA damage resulting from PCAF depletion. To investigate our hypothesis, we performed immunofluorescence and DNA–RNA immunoprecipitation (DRIP) assays using wild-type (WT) and PCAF KO cells with the S9.6 antibody, which is known to recognize R-loops (47–49). First, we quantified nuclear S9.6 signals across multiple cell panels. The nuclear S9.6 signal was observed in PCAF KO cells both in nucleoli and non-nucleoli regions, as indicated by the nucleoli marker (Figure 1E). We prominently observed the cytoplasmic S9.6 signal, suggesting that may originate from mitochondria and/or cytoplasmic RNA/DNA hybrids released by damage DNA (27,50). To check this hypothesis, we performed immunofluorescence (IF) experiments using the GFP-RNase H mutant. We found that the cytoplasmic RNA/DNA hybrids were increased in PCAF KO cells (Supplementary Figure S1C and D) which means that the damaged DNA were released to cytoplasm in PCAF KO cells. To confirm R-loop accumulation at specific *β-actin* loci, which are previously reported R-loop prone sites (28), we carried out the DRIP-qPCR assay in U2OS WT and PCAF KO cells. The R-loop levels were significantly increased in the indicated *β-actin* loci, and these signals were diminished by RNase H enzyme treatment (Supplementary Figure S1E). Importantly, we found that R-loop accumulation by PCAF loss was effectively suppressed by treatment with triptolide (Supplementary Figure S1F). We also checked the R-loop accumulation in different cell lines because the U2OS cell has an alternative lengthening of telomere (ALT). R-loops are formed at telomeric regions due to the transcription of telomeric repeat-containing RNA (TERRA) (51). TERRA RNA can invade telomeric dsDNA and form telomeric R-loop structures. To check whether this R-loop accumulation is dependent on

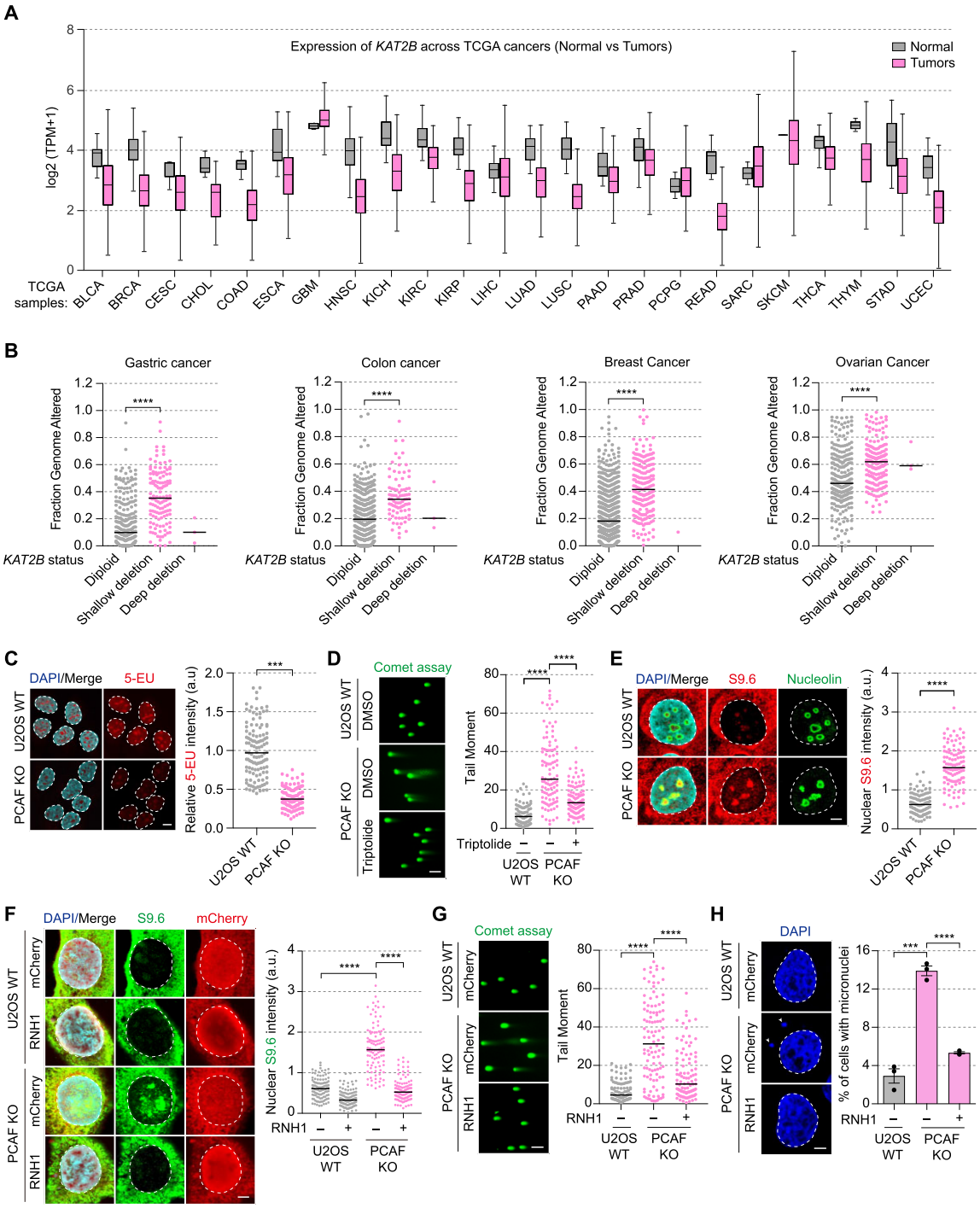

Figure 1. KAT2B (PCAF) is suppressed in human cancer, which accelerates genomic instability. (**A**) The pan-cancer analysis in the UALCAN database showed *KAT2B* expression in different cancers. (**B**) Fraction of Genome Altered in TCGA Gastric, Colon, Breast, Ovarian cohort. Black bars indicate the median and statistical significances were analyzed by two-tailed unpaired *t*-test. $^{****}P < 0.0001$. (**C**) Loss of PCAF suppresses the transcription process. The transcription level was confirmed by nascent 5-EU incorporation, and 5-EU intensity was normalized to the mean of the U2OS WT value. Representative images are shown in the left panel and quantification in the right panel (from >100 cells). $^{***}P < 0.001$. The scale bar indicates 10 μm. (**D**) Loss of PCAF triggers DNA breaks in a transcription-dependent manner. U2OS WT and PCAF KO cells were treated with transcription inhibitor (Triptolide; 1 μM, 3 h) and DNA breaks were monitored by neutral comet assay (left panel). Tail moments were calculated, and statistical analysis was performed by the Mann–Whitney test (right panel). The black bar indicates the median from >100 cells. $^{****}P < 0.0001$. Scale bar indicates 100 μm. (**E**) PCAF deficiency induces R-loops. R-loop levels were determined using immunofluorescence (IF) with S9.6 antibody (left panel). Nuclear S9.6 intensity was quantified by ImageJ and normalized to U2OS WT (right panel). The black bar indicates the median from > 100 cells. $^{****}P < 0.0001$. Scale bar indicates 5 μm. (**F**) IF images and quantification of WT and PCAF KO cells stained with S9.6 (green) and RNase H1 (mCherry). Diminution of the nuclear S9.6 signal by RNase H1 (RNH1) overexpression confirmed the signal specificity. Data analysis was performed as in Figure 1E. $^{****}P < 0.0001$. (**G**) DNA breaks in PCAF KO cells were generated by R-loop accumulation. DNA breaks were measured by neutral comet assay and representative images are shown in the left panel. Data was analyzed by the Mann–Whitney test for significance. Black bars indicate the median from >100 cells. $^{****}P < 0.0001$. The scale bar indicates 100 μm. (**H**) PCAF-mediated R-loop accumulation leads to genome instability. PCAF-deficient cells were analyzed for micronuclei formation in the presence or absence of RNase H1 (RNH1). Data represent the mean ± S.E.M. Scale bar indicated 5 μm.

TERRA, we checked the R-loop accumulation in non-ALT cell lines like RPE and MRC5. The R-loop accumulation and DNA damage were increased in PCAF knock down RPE and MRC5 cells (Supplementary Figure S2A–F).

The results showed that PCAF depletion triggers R-loop accumulation in cells, potentially causing endogenous DNA damage. Notably, the S9.6 antibody recognizes both RNA/DNA hybrids and double-stranded RNA (dsRNA) (52,53). To eliminate the possibility of this antibody detecting dsRNA, we introduced the R-loop-resolving enzyme RNase H1 into PCAF KO cells and then detected R-loop levels using immunofluorescence. Overexpression of mCherry-RNase H1 (RNH1) removed the nuclear R-loop signal in PCAF KO cells (Figure 1F and Supplementary Figure S3A). Furthermore, we validated these results using the S9.6 dot blot assay. Genomic DNA (gDNA) was purified from U2OS WT or PCAF KO cells and measured by dot blot assay with the S9.6 antibody. These S9.6 signal were also sensitive to RNase H (RNH) enzyme treatment (Supplementary Figure S3B). The disappearance of the R-loop signals following RNase H1 overexpression or RNase H enzyme treatment confirmed that it was a genuine R-loop signal. To directly establish that DNA damage and reduction of transcription rate were due to R-loop formation, we overexpressed RNase H1 in PCAF KO cells to eliminate the accumulated R-loops. We found that cells overexpressing RNase H1 exhibited fewer DSBs, as evidenced by a neutral comet assay (Figure 1G) and the transcription rates were restored to normal levels (Supplementary Figure S3C). Additionally, RNase H1 overexpression effectively inhibited micronuclei formation induced by DNA breaks (Figure 1H), thereby providing strong evidence that DNA damage resulting from PCAF depletion can be attributed to R-loop accumulation.

Transcriptional dysfunction can impede replication fork progression, causing collisions that collapse forks and induce DNA damage (54). Persistent R-loops formation induce unregulated transcription upon PCAF depletion led us to hypothesize that DNA damage arose from collisions with the replication machinery. To test this, we used the proximity ligation assay (PLA) to detect RNA pol II-PCNA interactions, indicating conflicts between transcription and replication. The PLA is a well-established *in situ* technique for detecting protein-protein interactions (55). PCAF knockout cells exhibited PLA foci (Supplementary Figure S3D and E), suggesting that deregulated transcription from PCAF loss causes DNA damage via transcription-replication collisions.

PCAF localizes to R-loop accumulated sites

Next, we sought to understand PCAF's involvement in R-loop resolution by examining its localization at R-loop accumulation sites. To achieve this, we employed customized proximity ligation assay (PLA) (30). We modified this approach to identify the interaction between R-loops and R-loop-interacting proteins using S9.6 and PCAF antibodies. We observed that no PLA foci were present in the S9.6-only or PCAF antibody-only groups. However, the S9.6/PCAF group exhibited numerous PLA foci, suggesting that endogenous PCAF is proximal to R-loop accumulation sites (Supplementary Figure S3F). Moreover, we confirmed this PCAF localization using R-loop immunoprecipitation (IP) (28). After extracting and sonicating the chromatin fraction, R-loop-interacting proteins were immunoprecipitated using the S9.6 antibody after RNase A trimming (Supplementary Figure S3G). We found that PCAF proteins were exclusively present in S9.6 immunoprecipitated samples but not in the IgG control (Supplementary Figure S3H). These data demonstrate that endogenous PCAF closely localizes to R-loop accumulation regions.

The recruitment of MRE11/EXO1 is necessary for PCAF at R-loop sites

Aberrant R-loops are regulated by nucleases, helicases, and FA proteins. Nucleases degrade RNA or DNA within R-loops (16,56), helicases unwind R-loop structures (14,57,58), and FA proteins suppress R-loops with RNA processing factors (4,59). To gain insight into the molecular mechanisms by which PCAF participates in R-loop resolution, we conducted a series of double depletions targeting PCAF along with one of the R-loop resolving enzymes (i.e. MRE11, EXO1, CtIP, SETX and FANCD2). The knockdown efficiency of the indicated siRNAs was confirmed using qRT-PCR (Supplementary Figure S4A). Subsequently, we assessed DNA breaks using a comet assay. As expected, the single depletion of any R-loop regulating factor increased the DNA damage in U2OS WT cells (Figure 2A). However, co-depletion of PCAF with CtIP, SETX or FANCD2 further elevated the number of DNA breakages, whereas MRE11- or EXO1-knockdown cells did not exhibit significant changes in PCAF KO cells compared with single depletion. Consistent with the comet assay, R-loop levels remained similar in both single- and double-depletion trials (Supplementary Figure S4B and C). The epistatic effects on DNA damage suggest that PCAF, MRE11 and EXO1 function in the same pathway for preventing R-loop accumulation and the associated DNA damage.

After identifying MRE11 and EXO1 as participants in PCAF-mediated R-loop resolution, we investigated whether PCAF is essential for their recruitment to R-loop accumulation sites using the R-loop IP assay (Supplementary Figure S4D). In PCAF KO cells, we observed a significant reduction in the interaction between MRE11, EXO1, and R-loops. To further assess the recruitment of MRE11 and EXO1 to the R-loop sites, we conducted a PLA assay using antibodies against MRE11, EXO1, and S9.6 antibodies. The recruitment of MRE11 and EXO1 was notably decreased in PCAF KO cells (Figure 2B and C). To examine whether PCAF can actively recruit these proteins to sites of aberrant R-loop accumulation, we treated topoisomerase I inhibitor (camptothecin, CPT), inducing the accumulation of aberrant R-loops on the chromosomes. Under these conditions, we observed a robust increase in MRE11 and EXO1 recruitment, which did not occur in PCAF KO cells. This finding suggests that PCAF is responsible for recruiting MRE11 and EXO1, thereby regulating both the normal and aberrant R-loop levels.

PCAF-mediated histone acetylation serves as a potentially crucial signal in preventing aberrant R-loop accumulation

Given the pivotal role of HAT activity in PCAF-mediated genome stability (11,12,20,60–62), we hypothesized that histone acetylation may be involved in R-loop resolution. We employed a complement assay in PCAF KO cells using a PCAF mutant with impaired HAT activity (i.e. YFAA). The conserved YF amino acids in the HAT domain were mutated to disrupt the HAT activity (63) (Figure 3A and B). PCAF KO

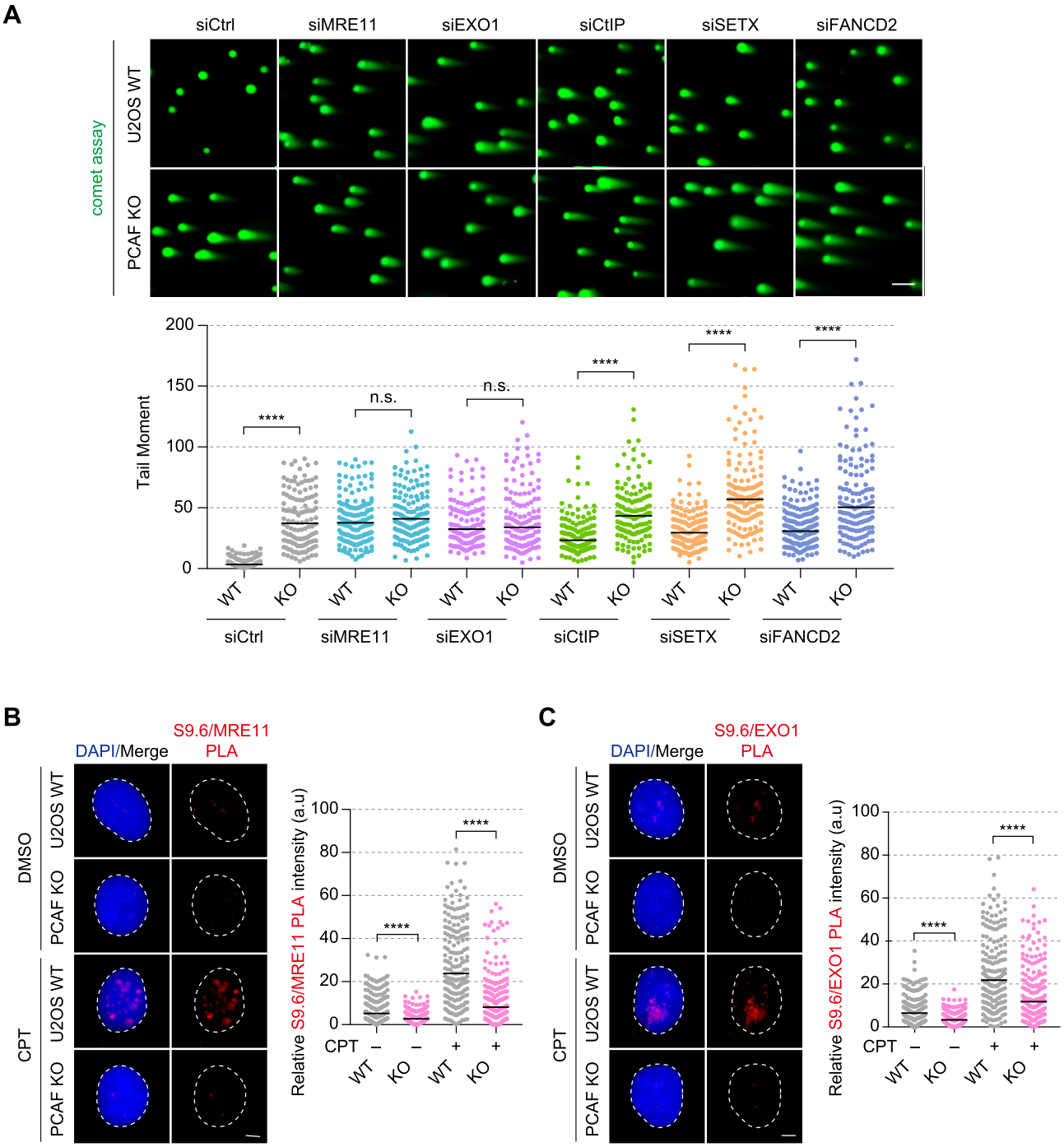

Figure 2. The recruitment of MRE11/EXO1 is necessary for PCAF at R-loop sites. (**A**) Functional analysis examined the relationship between PCAF and R-loop regulating factors. Cells were transfected with indicated siRNAs and then evaluated for DNA breaks by neutral comet assay. Black bars represent the median from >100 cells, with significance assessed by the Mann–Whitney test. $^{****}P < 0.0001$, n.s., not significant. Scale bar indicates 100 μm. (B, C) R-loop PLA assay with MRE11 (**B**) and EXO1 (**C**) antibodies. U2OS WT and PCAF KO cells were treated with CPT (10 μM, 2 h) and then subjected to a PLA assay to assess the physical closeness with the R-loop. The representative images are shown in the left panel, and the relative PLA intensity was quantified using ImageJ (right panel). Data were analyzed by the Mann–Whitney test for significance. Black bars indicate the median from >100 cells. $^{****}P < 0.0001$. The scale bar indicates 5 μm.

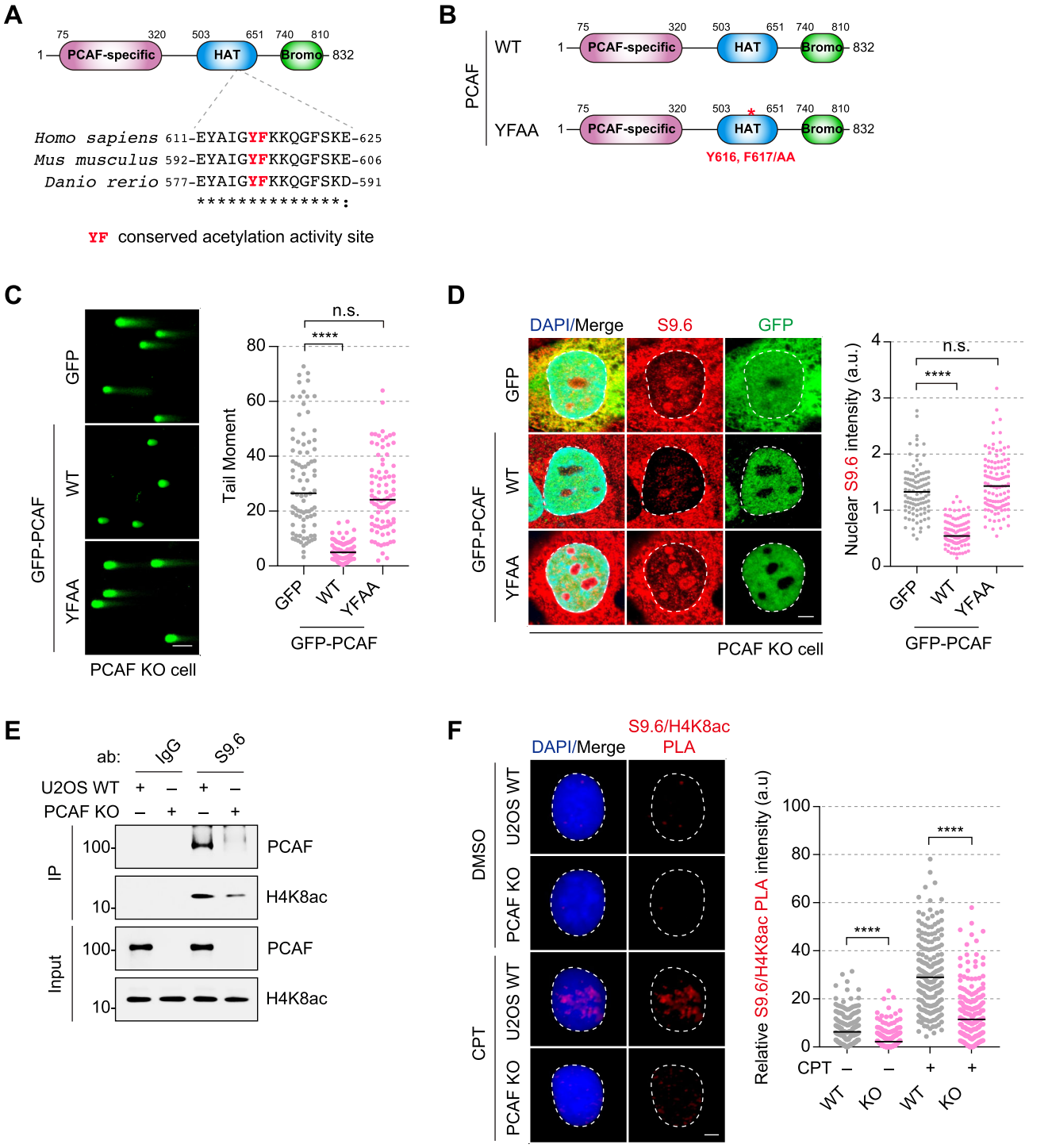

Figure 3. PCAF-mediated histone acetylation is required to prevent R-loop accumulation. (**A**) Diagram of PCAF domain structure. (**B**) Site-specific mutation of PCAF HAT domain (PCAF YFAA) for inhibiting acetylation activity. (**C**) Comet assay of PCAF KO cells expressing GFP-PCAF WT or catalytic inactive mutant (YFAA). PCAF KO Cells were transfected with GFP-tagged PCAF WT or YFAA, and DNA breaks were analyzed by neutral comet assay (left panel, quantified in the right panel). Statistical analysis of DNA breaks was carried out using the Mann–Whitney test (from >100 cells). ****$P < 0.0001$. n.s., not significant. The scale bar indicates 100 μm. (**D**) Acetylation activity of PCAF is necessary for R-loop resolution. GFP-PCAF WT and YFAA were transfected into PCAF KO cells and then stained with S9.6/GFP antibodies. The nuclear S9.6 intensity was measured using ImageJ, and statistical analysis was performed by the Mann–Whitney test (from >100 cells). ****$P < 0.0001$. n.s., not significant. Scale bar indicates 5 μm. (**E**) Western blotting for endogenous PCAF and H4K8ac after R-loop IP. U2OS WT and PCAF KO cells were harvested and immunoprecipitated with the S9.6 antibody. PCAF and H4K8ac levels were detected in the input and R-loop IP samples. IgG was used as IP control. (**F**) Evaluation of the H4K8ac levels in the R-loop site. PLA assay between S9.6 and H4K8ac was performed after CPT (10 μM, 2 h) treatment, and the relative PLA intensity was calculated by ImageJ. Data was analyzed by the Mann–Whitney test, and the black bar indicated the median from >100 cells. ****$P < 0.0001$. Scale bar indicates 5 μm.

cells were complemented with both PCAF WT and YFAA mutant, and we then assessed the levels of DNA damage and R-loop accumulation (Figure 3C and D). We found that while PCAF WT successfully restored DNA integrity and reduced R-loop accumulation, cells expressing the YFAA mutant continued to exhibit R-loop accumulation and DNA breakage, indicating endogenous DNA damage. These results strongly suggested that PCAF-mediated histone acetylation is critical for R-loop resolution. In our previous study, we demonstrated that PCAF acetylates H4K8 to recruit MRE11 and EXO1 at stalled replication forks (20). Based on this finding, we hypothesized that PCAF directly acetylates H4K8 at R-loop sites to recruit nucleases. To test this hypothesis, we assessed H4K8 acetylation levels at the R-loop sites using R-loop IP with S9.6 antibodies. Our observations revealed the downregulation of H4K8ac levels at R-loop sites in PCAF KO cells, despite the H4K8ac levels were not significantly reduced in the input sample (Figure 3E). Moreover, following treatment with topoisomerase I inhibitor (CPT), sites with aberrant R-loop accumulation on chromosomes also exhibited increased H4K8 acetylation (Figure 3F). Taken together, histone H4K8 acetylation by PCAF was markedly increased in the context of R-loop accumulation, indicating its potential role as a crucial signal for R-loop resolution.

H4K8 acetylation promotes the recruitment of MRE11 and EXO1 at R-loop region for R-loop resolution

To investigate how H4K8ac recruits MRE11 and EXO1 to the R-loop sites, we initially generated a binding mutant of H4K8ac for MRE11 and EXO1 (Figure 4A and E). In our previous study, we found that MRE11 and EXO1 directly bind to H4K8ac *via* their DNA-binding and PIN domains, respectively (20). Using these mutants, we investigated the recruitment of both WT and H4K8ac binding mutant of MRE11 or EXO1 to the R-loop sites. To prevent dimerization with endogenous proteins, we established knockdown cell lines for MRE11 or EXO1 using shRNA targeting their untranslated regions (UTRs). The efficacy of this knockdown was confirmed by western blotting (Supplementary Figure S5A and B), and we also confirmed that the WT and mutant forms of MRE11 or EXO1 were ectopically expressed in these shRNA-mediated knockdown cells (Supplementary Figure S5C and D). We next set out to determine the recruitment of H4K8ac binding mutant to the R-loop sites. Therefore, we investigated whether the binding activity of H4K8ac is a requisite factor for the assembly of MRE11/EXO1 in the R-loop region. To address this question, we performed co-immunoprecipitation experiments using S9.6 antibody in MRE11- or EXO1-deficient cells with WT or mutant overexpression. Interestingly, H4K8ac binding mutants (MRE11-Δ1, EXO1-ΔPIN) were not recruited to the R-loop region, whereas WT was enriched in the R-loop region (Figure 4B and F). Similar results were obtained by the PLA assay, which showed that H4K8ac binding mutants exhibited impaired binding to aberrant R-loops following CPT treatment (Figure 4C and G). Thus, we measured R-loop levels in WT and H4K8ac binding mutant-complemented cells using a dot blot assay (Figure 4D and H). As anticipated, MRE11 or EXO1 WT effectively suppressed R-loop accumulation, whereas this accumulation was still observed in the H4K8ac binding mutant, similar to endogenous MRE11 and EXO1 KO cells. These data suggest the significance of H4K8ac binding to MRE11 and EXO1 in resolving the R-loops. Therefore, we speculate that these nucleases must bind to the PCAF-generated histone mark, H4K8ac, to maintain their normal association and activity at R-loop sites.

The nucleolytic activity of EXO1 is dispensable for R-loop resolution

MRE11 and EXO1 play dual roles since they provide both catalytic and structural functions in facilitating DNA repair during DNA DSBs. Their catalytic activity involves the direct resection of broken DNA for efficient homologous recombination (HR) repair, as demonstrated in previous studies (64–66). Their structural activity promotes HR repair through interactions with helicase proteins like BLM (67), by binding to WRN (68), or by activating the Fanconi anemia (FA) pathway (69). Although the catalytic activity of MRE11 is not required for resolving R-loops (16), the role of EXO1 in this context remains unknown. To assess the importance of the catalytic activity of EXO1 for R-loop resolution, we compared R-loop accumulation in cells overexpressing WT or catalytic mutant. Prior to this test, we verified the relative activity levels of the catalytic mutants using a nuclease assay (Supplementary Figure S6A–D). we engineered a catalytic-dead mutant (CM) for MRE11 (H129N) and EXO1 (D173A) using site-directed mutagenesis, and purified recombinant proteins for both WT and CM forms of MRE11 and EXO1. Specifically, MRE11 was purified by utilizing the MRE11-Rad50 complex to assess its protein activity (33) and the purified proteins were confirmed using Coomassie Brilliant Blue staining (Supplementary Figure S4A and C). We then performed a nuclease assay on a 3′-overhang double-stranded DNA (dsDNA) oligonucleotide conjugated with 5′-Cy3. The results showed that WT proteins for MRE11 and EXO1 efficiently cleaved the 20-nt dsDNA, whereas catalytic mutants (CM) exhibited a complete absence of nuclease activity (Supplementary Figure S4B and D). Subsequently, we transfected the WT and CM forms of MRE11 and EXO1 into shRNA-mediated knockdown cells (Supplementary Figure S6E and G) and conducted a dot blot assay to assess R-loop resolution using catalytic activity. The findings indicated that EXO1 catalytically dead mutant also removed the accumulated R-loop, similar to WT. These results showed that the catalytic activity of EXO1 is not necessary for R-loop resolution, like MRE11 (Supplementary Figure S6F and H). Furthermore, we investigated the nucleolytic activities of MRE11 and EXO1 against double-stranded DNA (dsDNA), RNA/DNA hybrids, and R-loops (Supplementary Figure S7A and B). To conduct this experiment, we synthesized 5′-Cy3-conjugated dsDNA, RNA/DNA hybrid, and R-loop. MRE11 and EXO1 efficiently cleaved both dsDNA and RNA/DNA hybrid substrates, with substantial and complete degradation observed after 30 and 90 min, respectively. However, there was no observable degradation of the R-loop substrate by 30 or 90 min after incubation. These findings suggest that, while catalytic activity is dispensable for R-loop resolution, structural activity may be important for MRE11- and EXO1-mediated R-loop resolution.

PCAF recruits Fanconi anemia (FA)-associated helicases to the R-loop site

MRE11 and EXO1 collaborate with helicases and FA proteins involved in the DSB repair pathway, and these heli-

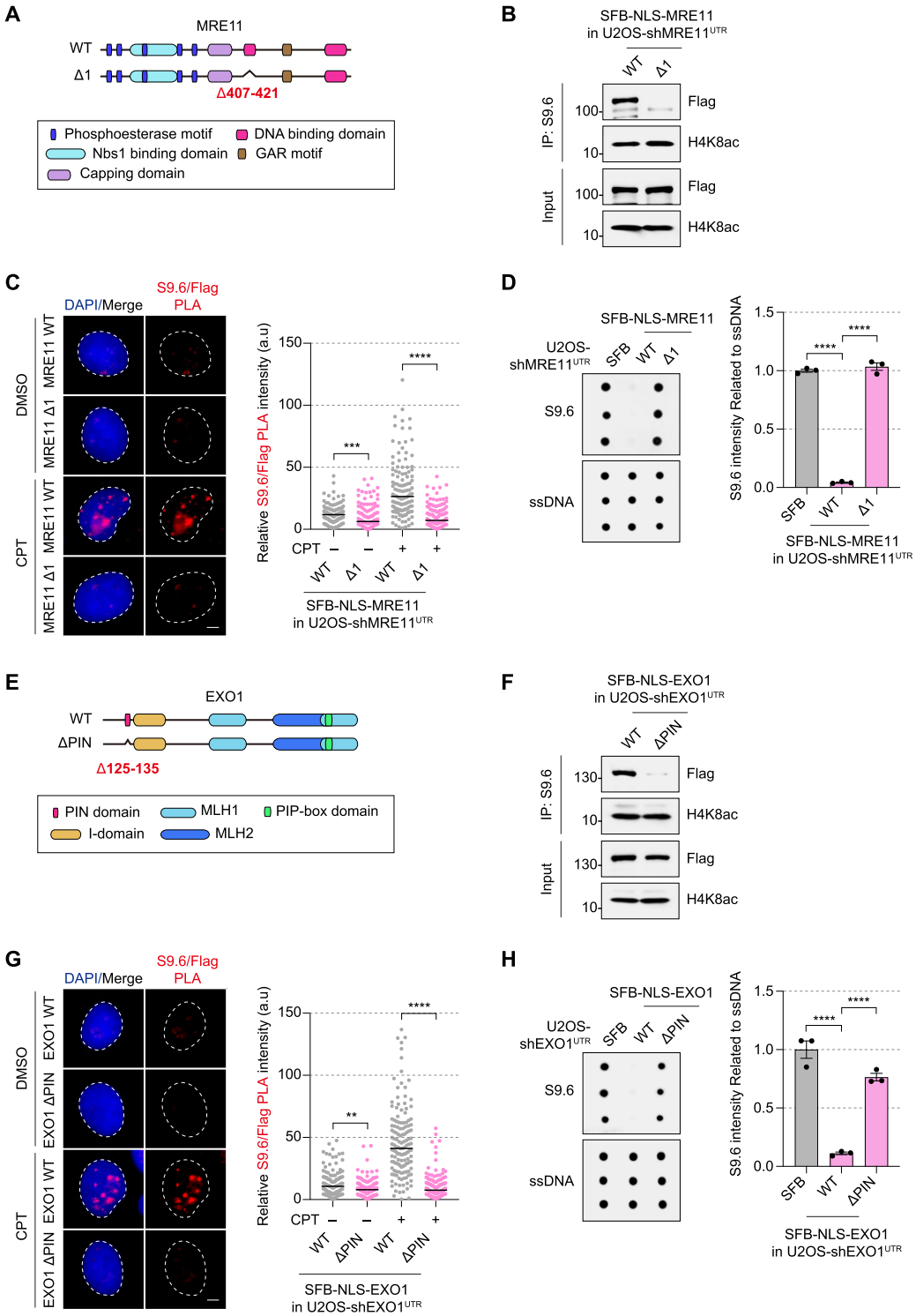

Figure 4. MRE11 and EXO1 were recruited to R-loop sites through binding to H4K8ac. (**A**) Schematic illustrations of MRE11 WT and mutant (H4K8ac binding mutant; △1). (**B**) Analysis of the interaction with the R-loop was conducted using MRE11 WT or mutant (H4K8ac binding mutant; △1). MRE11-deficient cells were transfected with SFB-NLS-MRE11 WT and mutant (△1), followed by immunoprecipitated with S9.6 antibody. The input and IP samples were detected using Flag and H4K8ac antibodies. (**C**) PLA assays were conducted between S9.6 and Flag-MRE11. Cells were transfected with SFB vectors for 24 h and changed with the new medium. Cells were further incubated and treated with DMSO or CPT (10 μM, 2 h) before PLA assay. Relative PLA intensity was analyzed using the Mann–Whitney test, and the black bar indicates the median from > 100 cells. $^{****}P < 0.0001$, $^{***}P < 0.001$, $^{**}P < 0.01$. The scale bar indicates 5 μm. (**D**) H4K8ac binding activity of MRE11 is required for R-loop resolution. R-loop levels were analyzed by dot blot assay against anti-S9.6 and quantified. Parallel ssDNA dot blots provided a loading control, and the S9.6 signal was normalized to ssDNA level and EV control. Statistical significances were analyzed by a two-tailed unpaired *t*-test (mean ± S.E.M.). $^{****}P < 0.0001$. (**E**) Domain diagram of EXO1 WT and H4K8ac binding mutant (△PIN). (**F**) R-loop IP was performed for EXO1 WT and mutant (H4K8ac binding mutant; △PIN). EXO1-depleted cells were transfected with SFB-NLS EXO1 (WT or mutant) and harvested for R-loop IP. The recruitment of EXO1 to R-loop sites was observed using western blotting against anti-Flag and anti-H4K8ac. (**G**) PLA assay was performed in EXO1-deficient cells and analyzed as in Figure 4C. (**H**) The R-loop levels were assessed using a dot blot assay. EXO1-depleted cells were transfected with the indicated SFB vectors and analyzed as in Figure 4D.

cases and FA proteins may be involved in resolving R-loops. For example, helicase FANCM has been proposed as a direct effector of R-loops, since it has demonstrated the capability to unwind them *in vitro* (70). FANCM functions as an anchor and is essential for nuclear localization of BLM following replication stalling (71). Since BLM, another helicase, has been shown to affect R-loop accumulation (13), these proteins are clearly important for R-loop resolution. Previously, Chang *et al*. demonstrated the essential role of the MRN complex in recruiting FANCM and BLM to R-loop-prone sites independent of its catalytic activity (16). However, the role of EXO1 in recruiting these proteins remains unknown. To understand how EXO1 influences the recruitment of FANCM and BLM to R-loops, we performed chromatin immunoprecipitation and quantitative real-time PCR (ChIP-qPCR) to demonstrate that the binding of FANCM and BLM to R-loop-prone loci (*β-actin*, *BTBD19*, *TFPT*) (16,28) when either MRE11 or EXO1 was depleted (Figure 5A–D). The FANCM and BLM protein levels are not altered by MRE11 and EXO1 knockdown (Supplementary Figure S7C). These results indicate that both MRE11 and EXO1 are required for efficient recruitment of FANCM and BLM to R-loop sites. In addition, our findings suggest that PCAF might affect FANCM/BLM recruitment *via* the MRE11 and EXO1 axis. To further understand how PCAF mediates FANCM/BLM recruitment to R-loops *via* MRE11 and EXO1, we conducted PLA and ChIP-qPCR assays to evaluate FANCM/BLM recruitment to R-loops in PCAF KO cells. The PLA assay revealed decreased recruitment of FANCM and BLM at R-loop accumulation sites in both DMSO- and CPT-treated PCAF KO cells (Figure 5E and F). Furthermore, the recruitment of these proteins to R-loop-prone sites (*β-actin*, *BTBD19*, *TFPT*) was also reduced in PCAF KO cells (Figure 5G–J). Taken together, these results highlight the critical role of the PCAF-MRE11/EXO1-FANCM/BLM axis in R-loop resolution.

PCAF can remove pathogenic R-loops in BRCA1- or SETX-depleted cells

Excess accumulation of R-loops has been observed in various human diseases, including neurological disorders and cancer (72,73). The latter is not surprising, since R-loops are known to contribute to genome instability and replication stress, which are two characteristic features of tumor cells (74). Well-known tumor suppressor genes, such as BRCA, are known to undergo extensive mutations in various cancers, including breast, ovarian, gastric, and pancreatic cancers (75–79). Heterozygous germline mutations in either BRCA1 or BRCA2, which impair normal function, significantly elevate the risk of these cancers, particularly due to the loss of BRCA WT alleles during tumorigenesis. Consequently, cells depleted of BRCA1 or BRCA2 are known to accumulate R-loops and experience R-loop-dependent DNA breakages (57,80). Senataxin (SETX), an RNA/DNA helicase, has been implicated in transcriptional regulation and the DNA damage response by resolving R-loop structures (81). Mutations in SETX have also been identified in major neurodegenerative disorders. For example, dominant mutations in SETX result in a juvenile form of amyotrophic lateral sclerosis, known as ALS4, while recessive mutations are responsible for ataxia, specifically forms of ataxia associated with oculomotor apraxia type 2 (AOA2) (82,83). SETX knockdown (KD) can increase significant DSB-induced R loop-dependent deletions near the site of the breakage (84). Finally, AOA2- or SETX-depleted cells have also been associated with increased incidence of R-loops and DSBs. To investigate whether the PCAF-MRE11/EXO1-FANCM/BLM axis unwinds R-loops under pathological conditions, we examined the impact of PCAF overexpression on R-loop accumulation induced by BRCA1- or SETX-depletion in U2OS cells. Dot blot assays and S9.6 IF assays revealed increased levels of R-loop accumulation in BRCA1- or SETX-depleted cells, while PCAF effectively suppressed R-loop accumulation induced by BRCA1 or SETX depletion (Figure 6A–D). Conversely, cells overexpressing HAT-deficient mutant YFAA did not exhibit R-loop suppression (Figure 6A–D). Consistent with other data regarding R-loop accumulation, the comet assay results demonstrated that overexpression of PCAF, but not the YFAA mutant, suppressed R-loop-mediated DNA breakages caused by BRCA1 or SETX depletion (Figure 6E and F). By overexpression of PCAF WT increased H4K8ac levels in total and R-loop prone sites but not YFAA mutant (Supplementary Figure S8A–D). Taken together, these data indicate that the PCAF-mediated H4K8ac-induced MRE11/EXO1-FANCM/BLM axis is crucial for resolving the pathological R-loop accumulation (Figure 7).

Discussion

DNA damage events can arise randomly or in a targeted manner during mRNA synthesis. In the absence of external genotoxic insults, normal transcription can trigger the formation of DSBs through R-loop generation (85). However, the pathological accumulation of R-loops results in genome instability, which in turn contributes to cancer development, tumorigenesis, cancer progression, and chemoresistance (5). R-loop-mediated genome instability has been extensively explored in blood cancers, including myelodysplastic syndrome and acute lymphoblastic leukemia (86), and in BRCA deficient cancers (87–90). Here, we found that diminished expression of PCAF, a HAT protein, in various cancers leads to abnormal R-loop accumulation, which suggested that PCAF plays a protective role in mitigating transcription-mediated endogenous DNA damage. Recent research has indicated that DNA DSB repair proteins, such as the MRE11–NBS1–RAD50 (MRN) complex, inhibit the formation of R-loops and associated DNA damage (16), which suggests that DSB proteins safeguard against endogenous DNA damage during transcription. However, the mechanisms underlying their recruitment to sites with accumulated R-loops remain unclear. In this context, our findings elucidate that histone acetylation by PCAF is a critical factor for promoting R-loop suppression and that this process occurs *via* the recruitment of MRE11 and EXO1 to R-loop accumulation sites.

Our study reveals that the nuclease activities of MRE11 and EXO1 are not necessary for the resolution of R-loops. This conclusion aligns with previous research by Chang *et al*. (16), which demonstrated that MRE11-mediated resection of RNA/DNA hybrids was less effective than DNA/DNA hybrids. Another study showed that structure-specific endonucleases, including XPF, XPG, FEN1 or MRE11, reduced the induction of γH2AX and 53BP1 foci upon CPT treatment (91). We observed that MRE11 did not directly cleave R-loop structures, similar to its inability to cleave RNA/DNA hybrids efficiently. These findings suggest that the nuclease-independent functions of MRE11 contribute to R-loop resolution. Additionally, we found that EXO1-mediated suppres-

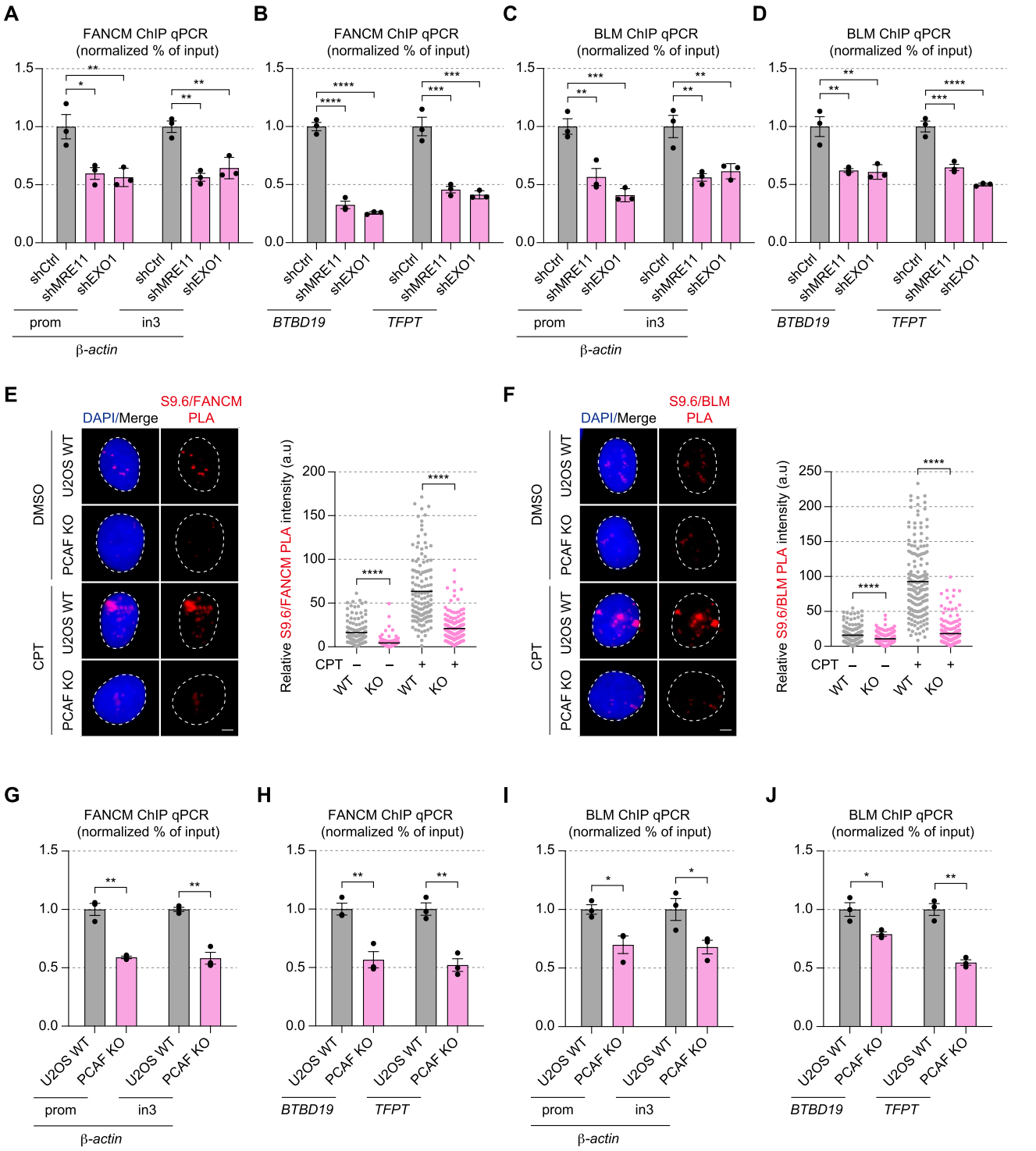

Figure 5. PCAF recruits Fanconi Anemia (FA)-associated helicases to the R-loop site. (**A–D**) The recruitment of FANCM (**A** and **B**) and BLM (**C** and **D**) was analyzed by ChIP-qPCR assay at R-loop prone loci (β-*actin*, *BTBD19* and *TFPT*) in MRE11 or EXO1 knockdown cells. Data are presented as mean ± S.E.M. ($N = 3$) and statistical significance is indicated as $^{****}P < 0.0001$, $^{***}P < 0.001$, $^{**}P < 0.01$, $^{*}P < 0.05$. (E, F) Representative images and quantification of the R-loop PLA assay. Cells were treated with either DMSO or CPT (10 μM, 2 h), and PLA foci were detected (**E**, FANCM; **F**, BLM). Relative PLA intensity was analyzed using the Mann–Whitney test, and the black bar indicates the median from > 100 cells. $^{****}P < 0.0001$. The scale bar indicates 5 μm. (G–J) The recruitment of FANCM and BLM was analyzed by ChIP-qPCR assay at R-loop prone loci (β-*actin*, *BTBD19* and *TFPT*). ChIP assays were performed in U2OS WT and PCAF KO cells, and immunoprecipitation was carried out using FANCM (**G** and **H**) or BLM (**I** and **J**) antibodies. Data are presented as mean ± S.E.M.; $N = 3$. $^{**}P < 0.01$, $^{*}P < 0.05$.

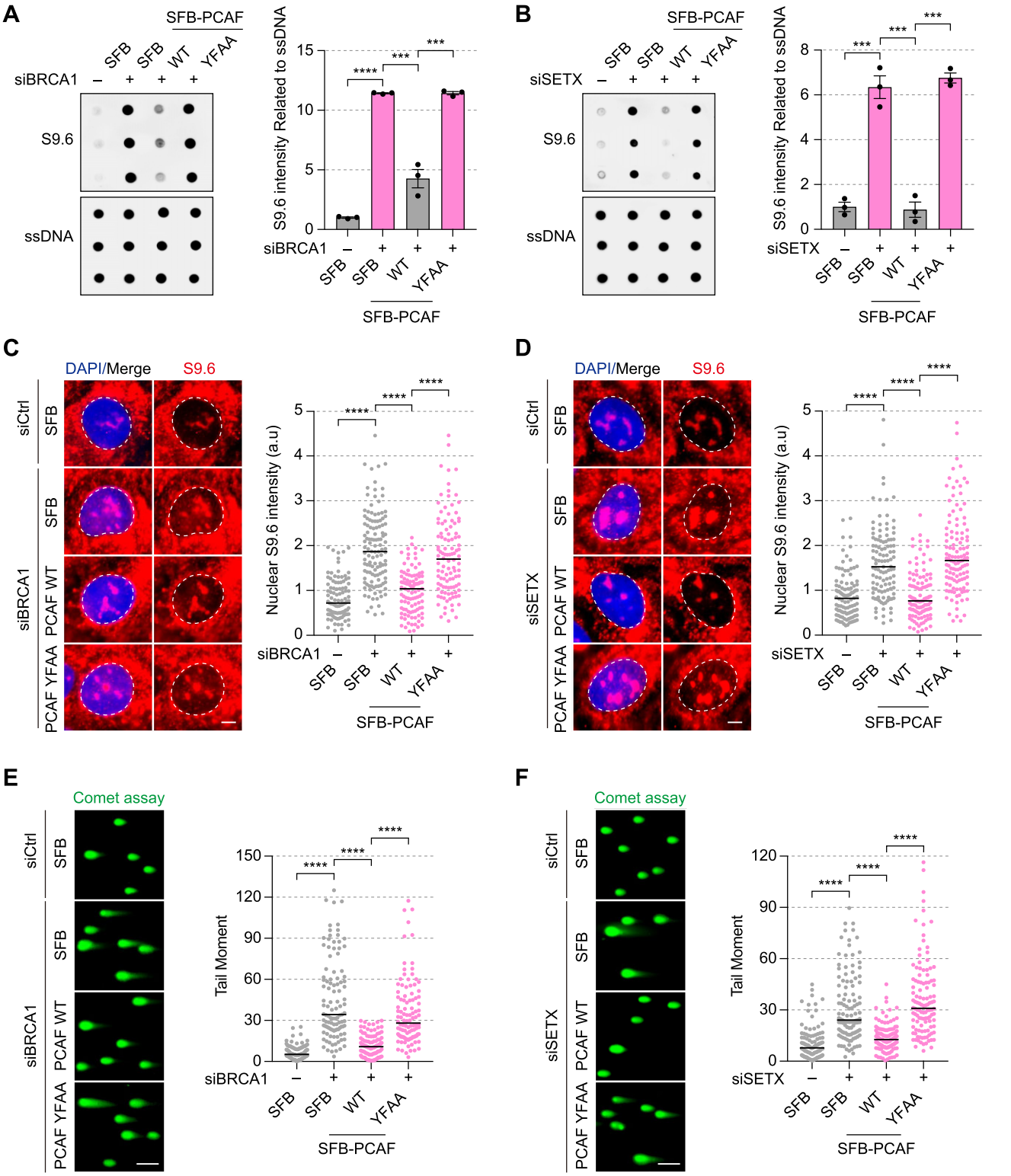

Figure 6. PCAF can remove pathogenic R-loops in BRCA1-, SETX-depleted cells. (A, B) Dot blot assays were performed for PCAF WT or YFAA overexpressed cells. The R-loop levels were assessed following the knockdown of BRCA1 (**A**) or SETX (**B**) and overexpression of PCAF WT or YFAA. R-loop signal was detected using the S9.6 antibody and quantified. The normalization of S9.6 intensity was performed relative to ssDNA levels and siCtrl-EV control. Statistical significances were analyzed using a two-tailed unpaired *t*-test. $^{****}P < 0.0001$. $^{***}P < 0.001$. (**C, D**) R-loop levels were detected by S9.6 IF and quantified. Cells were transfected with siRNA for BRCA1 or SETX and the expression vector for WT or YFAA mutant of PCAF. Nuclear R-loops were captured using IF with S9.6 antibody (left panel) and intensity was quantified by ImageJ (right panel). Data represents the median from >100 cells and statistical significance was analyzed by the Mann–Whitney test. $^{****}P < 0.0001$. The scale bar indicates 5 μm. (E, F) DNA breaks were measured by neutral comet assay after BRCA1 (**E**) or SETX (**F**) knockdown. Cells were transfected with the expression vector for SFB-tagged PCAF WT or YFAA mutant with siRNA against BRCA1 or SETX. Tail moments were analyzed by the Mann–Whitney test and black bars represent the median from >100 cells. $^{****}P < 0.0001$. The scale bar indicates 100 μm.

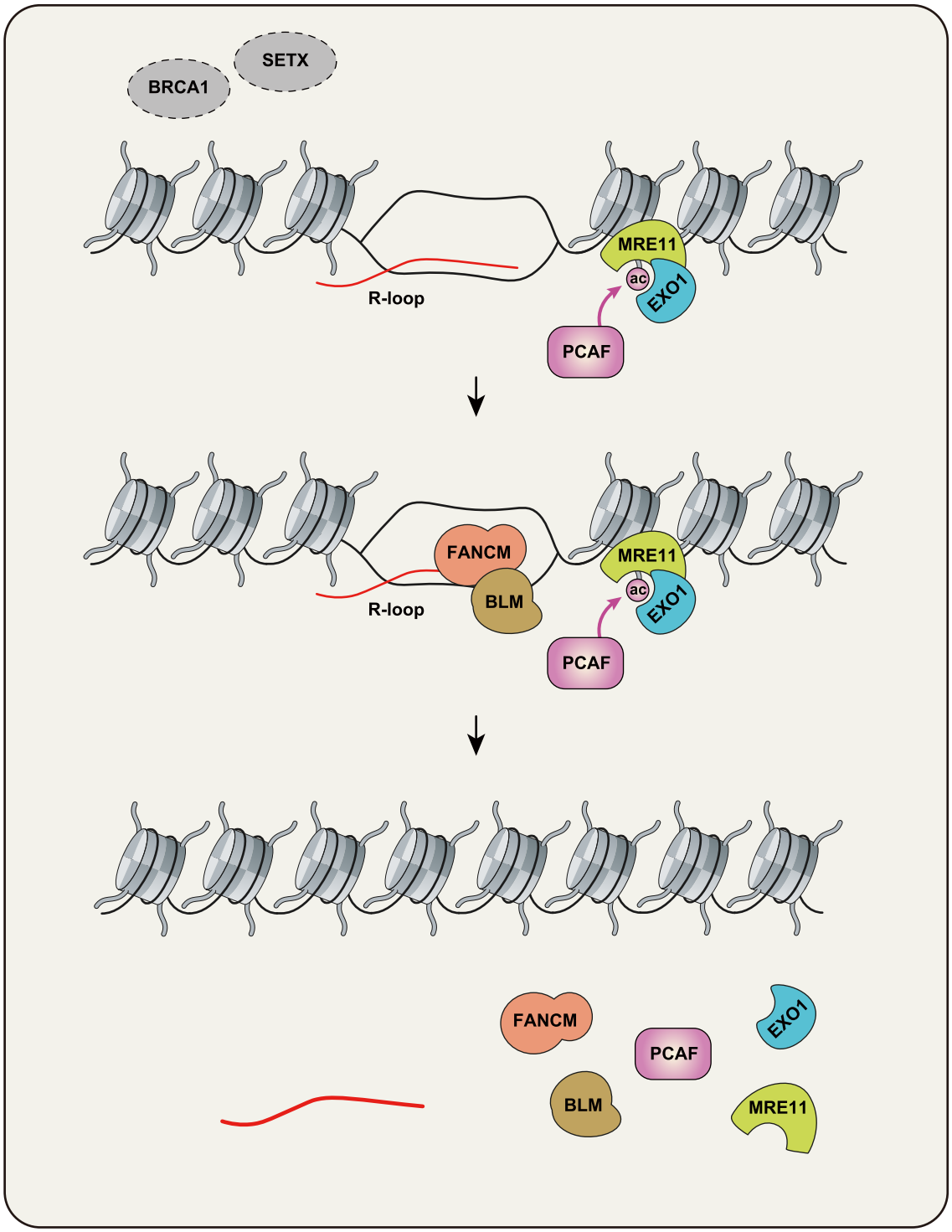

Figure 7. Model for PCAF mediated R-loop resolution. Histone acetyltransferase PCAF is responsible for acetylating histone H4K8, which facilitates the recruitment of MRE11 and EXO1 to R-loop sites. The recruitment of these proteins then leads to the recruitment of Fanconi anemia proteins FANCM and BLM, which act as a helicase to unwind the RNA-DNA hybrid structure. The coordinated actions of these proteins, facilitated by PCAF-mediated histone acetylation, prevent genome instability caused by unresolved R-loops.

sion of R-loop formation occurred independently of its nuclease function, like MRE11. This observation implies that both MRE11 and EXO1 may participate in R-loop resolution through shared nuclease-independent mechanisms. However, further investigations are needed to elucidate these mechanisms and the potential interplay between MRE11 and EXO1 in this process.

The elucidation of PCAF's role in resolving R-loops deepens our understanding of genome stability mechanisms and opens up promising avenues for therapeutic development. Targeting PCAF and its associated pathways has the potential to rectify aberrant R-loop accumulation, offering novel strategies to combat diseases linked to genome instability like cancer. In this work, we demonstrated that PCAF can remove the pathogenic R-loops in cells depleted of BRCA1 and SETX, implicating that PCAF activators might be good candidates for treating R-loop mediated diseases. These insights pave the way for developing precision therapies aimed at restoring cellular homeostasis and halting disease progression. By unravelling the intricate interplay between PCAF, histone acetylation, and Fanconi anemia proteins in maintaining genome stability, this study provides a compelling account of the molecular underpinnings of cellular health. Shedding light on the mechanisms governing R-loop resolution advances our fundamental understanding of genome stability dynamics while also holding profound therapeutic implications.

Data availability

The data analyzed during the current study are available from the corresponding author upon reasonable request.

Supplementary data

Supplementary Data are available at NAR Online.

Acknowledgements

We thank the Kim and Miller lab for their discussion of this study and acknowledge the funds from the National Research Foundation of Korea (NRF) of Korea government.

Author contributions: S.Y.L. and J.J.K. conceived and designed the project. S.Y.L. performed all the experiments unless otherwise noted. S.H.L. and J.Y.K. purified recombinant proteins and performed *in vitro* resection assay. S.H.L., N.H.C. and J.H.K. purified genomic DNA for dot blot assay. J.J.K. supervised this study and provided funding. K.M.M. contributed to deep discussion and comments. S.Y.L. and J.J.K. analyzed the data and wrote the manuscript. All authors have read and agreed to the published version of the manuscript.

Funding

National Research Foundation of Korea (NRF) grant funded by the Korea government (MIST) [NRF-2022R1C1C1007759, RS-2023-00217013 to J.J.K.]; National Cancer Institute grant (RO1 CA198279 and CA250905 to K.M.M.). Funding for open access charge: National Research Foundation of Korea (NRF) of Korea government.

Conflict of interest statement

None declared.

References

1. Garcia-Muse,T. and Aguilera,A. (2019) R loops: from physiological to pathological Roles. *Cell*, **179**, 604–618.
2. Santos-Pereira,J.M. and Aguilera,A. (2015) R loops: new modulators of genome dynamics and function. *Nat. Rev. Genet.*, **16**, 583–597.
3. Marnef,A. and Legube,G. (2021) R-loops as Janus-faced modulators of DNA repair. *Nat. Cell Biol.*, **23**, 305–313.
4. Petermann,E., Lan,L. and Zou,L. (2022) Sources, resolution and physiological relevance of R-loops and RNA-DNA hybrids. *Nat. Rev. Mol. Cell Biol.*, **23**, 521–540.
5. Wells,J.P., White,J. and Stirling,P.C. (2019) R Loops and their composite cancer connections. *Trends Cancer*, **5**, 619–631.
6. Nowotny,M., Gaidamakov,S.A., Ghirlando,R., Cerritelli,S.M., Crouch,R.J. and Yang,W. (2007) Structure of human RNase H1 complexed with an RNA/DNA hybrid: insight into HIV reverse transcription. *Mol. Cell*, **28**, 264–276.
7. Rychlik,M.P., Chon,H., Cerritelli,S.M., Klimek,P., Crouch,R.J. and Nowotny,M. (2010) Crystal structures of RNase H2 in complex with nucleic acid reveal the mechanism of RNA-DNA junction recognition and cleavage. *Mol. Cell*, **40**, 658–670.
8. Li,X. and Manley,J.L. (2005) Inactivation of the SR protein splicing factor ASF/SF2 results in genomic instability. *Cell*, **122**, 365–378.
9. Nguyen,H.D., Leong,W.Y., Li,W., Reddy,P.N.G., Sullivan,J.D., Walter,M.J., Zou,L. and Graubert,T.A. (2018) Spliceosome mutations induce R loop-associated sensitivity to ATR inhibition in myelodysplastic syndromes. *Cancer Res.*, **78**, 5363–5374.
10. El Hage,A., French,S.L., Beyer,A.L. and Tollervey,D. (2010) Loss of topoisomerase I leads to R-loop-mediated transcriptional blocks during ribosomal RNA synthesis. *Genes Dev.*, **24**, 1546–1558.
11. Kim,J.J., Lee,S.Y., Gong,F., Battenhouse,A.M., Boutz,D.R., Bashyal,A., Refvik,S.T., Chiang,C.M., Xhemalce,B., Paull,T.T., *et al.* (2019) Systematic bromodomain protein screens identify homologous recombination and R-loop suppression pathways involved in genome integrity. *Genes Dev.*, **33**, 1751–1774.
12. Lee,S.Y., Kim,J.J. and Miller,K.M. (2021) Bromodomain proteins: protectors against endogenous DNA damage and facilitators of genome integrity. *Exp. Mol. Med.*, **53**, 1268–1277.
13. Chang,E.Y., Novoa,C.A., Aristizabal,M.J., Coulombe,Y., Segovia,R., Chaturvedi,R., Shen,Y., Keong,C., Tam,A.S., Jones,S.J.M., *et al.* (2017) RECQ-like helicases Sgs1 and BLM regulate R-loop-associated genome instability. *J. Cell Biol.*, **216**, 3991–4005.
14. Cohen,S., Puget,N., Lin,Y.L., Clouaire,T., Aguirrebengoa,M., Rocher,V., Pasero,P., Canitrot,Y. and Legube,G. (2018) Senataxin resolves RNA:DNA hybrids forming at DNA double-strand breaks to prevent translocations. *Nat. Commun.*, **9**, 533.
15. Pan,X., Chen,Y., Biju,B., Ahmed,N., Kong,J., Goldenberg,M., Huang,J., Mohan,N., Klosek,S., Parsa,K., *et al.* (2019) FANCM suppresses DNA replication stress at ALT telomeres by disrupting TERRA R-loops. *Sci. Rep.*, **9**, 19110.
16. Chang,E.Y., Tsai,S., Aristizabal,M.J., Wells,J.P., Coulombe,Y., Busatto,F.F., Chan,Y.A., Kumar,A., Dan Zhu,Y., Wang,A.Y., *et al.* (2019) MRE11-RAD50-NBS1 promotes Fanconi anemia R-loop suppression at transcription-replication conflicts. *Nat. Commun.*, **10**, 4265.
17. Paull,T.T. (2018) 20 Years of Mre11 biology: no end in sight. *Mol. Cell*, **71**, 419–427.
18. Brickner,J.R., Garzon,J.L. and Cimprich,K.A. (2022) Walking a tightrope: the complex balancing act of R-loops in genome stability. *Mol. Cell*, **82**, 2267–2297.
19. D'Alessandro,G., Whelan,D.R., Howard,S.M., Vitelli,V., Renaudin,X., Adamowicz,M., Iannelli,F., Jones-Weinert,C.W., Lee,M., Matti,V., *et al.* (2018) BRCA2 controls DNA:RNA hybrid level at DSBs by mediating RNase H2 recruitment. *Nat. Commun.*, **9**, 5376.
20. Kim,J.J., Lee,S.Y., Choi,J.H., Woo,H.G., Xhemalce,B. and Miller,K.M. (2020) PCAF-mediated histone acetylation promotes

replication fork degradation by MRE11 and EXO1 in BRCA-deficient cells. *Mol. Cell*, **80**, 327–344.
21. Nagy,Z. and Tora,L. (2007) Distinct GCN5/PCAF-containing complexes function as co-activators and are involved in transcription factor and global histone acetylation. *Oncogene*, **26**, 5341–5357.
22. Zheng,X., Gai,X., Ding,F., Lu,Z., Tu,K., Yao,Y. and Liu,Q. (2013) Histone acetyltransferase PCAF up-regulated cell apoptosis in hepatocellular carcinoma via acetylating histone H4 and inactivating AKT signaling. *Mol. Cancer*, **12**, 96.
23. Love,I.M., Sekaric,P., Shi,D., Grossman,S.R. and Androphy,E.J. (2012) The histone acetyltransferase PCAF regulates p21 transcription through stress-induced acetylation of histone H3. *Cell Cycle*, **11**, 2458–2466.
24. Liu,T., Wang,X., Hu,W., Fang,Z., Jin,Y., Fang,X. and Miao,Q.R. (2019) Epigenetically Down-regulated acetyltransferase PCAF increases the resistance of colorectal cancer to 5-fluorouracil. *Neoplasia*, **21**, 557–570.
25. Malatesta,M., Steinhauer,C., Mohammad,F., Pandey,D.P., Squatrito,M. and Helin,K. (2013) Histone acetyltransferase PCAF is required for Hedgehog-Gli-dependent transcription and cancer cell proliferation. *Cancer Res.*, **73**, 6323–6333.
26. Crossley,M.P., Brickner,J.R., Song,C., Zar,S.M.T., Maw,S.S., Chedin,F., Tsai,M.S. and Cimprich,K.A. (2021) Catalytically inactive, purified RNase H1: a specific and sensitive probe for RNA-DNA hybrid imaging. *J. Cell Biol.*, **220**, e202101092.
27. Crossley,M.P., Song,C., Bocek,M.J., Choi,J.H., Kousouros,J.N., Sathirachinda,A., Lin,C., Brickner,J.R., Bai,G., Lans,H., *et al.* (2023) R-loop-derived cytoplasmic RNA-DNA hybrids activate an immune response. *Nature*, **613**, 187–194.
28. Cristini,A., Groh,M., Kristiansen,M.S. and Gromak,N. (2018) RNA/DNA hybrid interactome identifies DXH9 as a molecular player in transcriptional termination and R-loop-associated DNA damage. *Cell Rep.*, **23**, 1891–1905.
29. Beghe,C. and Gromak,N. (2022) R-loop immunoprecipitation: a method to detect R-loop interacting factors. *Methods Mol. Biol.*, **2528**, 215–237.
30. Alagia,A., Ketley,R.F. and Gullerova,M. (2022) Proximity ligation assay for detection of R-loop complexes upon DNA damage. *Methods Mol. Biol.*, **2528**, 289–303.
31. Hamperl,S., Bocek,M.J., Saldivar,J.C., Swigut,T. and Cimprich,K.A. (2017) Transcription-replication conflict orientation modulates R-loop levels and activates distinct DNA damage responses. *Cell*, **170**, 774–786.
32. Sanz,L.A. and Chedin,F. (2019) High-resolution, strand-specific R-loop mapping via S9.6-based DNA-RNA immunoprecipitation and high-throughput sequencing. *Nat. Protoc.*, **14**, 1734–1755.
33. Myler,L.R., Soniat,M.M., Zhang,X., Deshpande,R.A., Paull,T.T. and Finkelstein,I.J. (2019) Purification and biophysical characterization of the Mre11-Rad50-Nbs1 complex. *Methods Mol. Biol.*, **2004**, 269–287.
34. Boleslavska,B., Oravetzova,A., Shukla,K., Nascakova,Z., Ibini,O.N., Hasanova,Z., Andrs,M., Kanagaraj,R., Dobrovolna,J. and Janscak,P. (2022) DDX17 helicase promotes resolution of R-loop-mediated transcription-replication conflicts in human cells. *Nucleic Acids Res.*, **50**, 12274–12290.
35. Choudhary,C., Kumar,C., Gnad,F., Nielsen,M.L., Rehman,M., Walther,T.C., Olsen,J.V. and Mann,M. (2009) Lysine acetylation targets protein complexes and co-regulates major cellular functions. *Science*, **325**, 834–840.
36. Eberharter,A. and Becker,P.B. (2002) Histone acetylation: a switch between repressive and permissive chromatin. Second in review series on chromatin dynamics. *EMBO Rep.*, **3**, 224–229.
37. Marmorstein,R. and Zhou,M.M. (2014) Writers and readers of histone acetylation: structure, mechanism, and inhibition. *Cold Spring Harb. Perspect. Biol.*, **6**, a018762.
38. Audia,J.E. and Campbell,R.M. (2016) Histone modifications and cancer. *Cold Spring Harb. Perspect. Biol.*, **8**, a019521.
39. Cohen,I., Poreba,E., Kamieniarz,K. and Schneider,R. (2011) Histone modifiers in cancer: friends or foes? *Genes Cancer*, **2**, 631–647.
40. Zhao,Z. and Shilatifard,A. (2019) Epigenetic modifications of histones in cancer. *Genome Biol.*, **20**, 245.
41. Bensaude,O. (2011) Inhibiting eukaryotic transcription: which compound to choose? How to evaluate its activity? *Transcription*, **2**, 103–108.
42. Belotserkovskii,B.P., Tornaletti,S., D'Souza,A.D. and Hanawalt,P.C. (2018) R-loop generation during transcription: formation, processing and cellular outcomes. *DNA Repair (Amst.)*, **71**, 69–81.
43. Costantino,L. and Koshland,D. (2015) The Yin and Yang of R-loop biology. *Curr. Opin. Cell Biol.*, **34**, 39–45.
44. Aguilera,A. and Garcia-Muse,T. (2012) R loops: from transcription byproducts to threats to genome stability. *Mol. Cell*, **46**, 115–124.
45. Crossley,M.P., Bocek,M. and Cimprich,K.A. (2019) R-loops as cellular regulators and genomic threats. *Mol. Cell*, **73**, 398–411.
46. Puget,N., Miller,K.M. and Legube,G. (2019) Non-canonical DNA/RNA structures during transcription-coupled double-strand break repair: roadblocks or bona fide repair intermediates? *DNA Repair (Amst.)*, **81**, 102661.
47. Bou-Nader,C., Bothra,A., Garboczi,D.N., Leppla,S.H. and Zhang,J. (2022) Structural basis of R-loop recognition by the S9.6 monoclonal antibody. *Nat. Commun.*, **13**, 1641.
48. Phillips,D.D., Garboczi,D.N., Singh,K., Hu,Z., Leppla,S.H. and Leysath,C.E. (2013) The sub-nanomolar binding of DNA-RNA hybrids by the single-chain Fv fragment of antibody S9.6. *J. Mol. Recognit.*, **26**, 376–381.
49. Skourti-Stathaki,K. (2022) Detection of R-loop structures by immunofluorescence using the S9.6 monoclonal antibody. *Methods Mol. Biol.*, **2528**, 21–29.
50. Brown,T.A., Tkachuk,A.N. and Clayton,D.A. (2008) Native R-loops persist throughout the mouse mitochondrial DNA genome. *J. Biol. Chem.*, **283**, 36743–36751.
51. Gong,Y. and Liu,Y. (2023) R-loops at chromosome ends: from formation, regulation, and cellular consequence. *Cancers (Basel)*, **15**, 2178.
52. Hartono,S.R., Malapert,A., Legros,P., Bernard,P., Chedin,F. and Vanoosthuyse,V. (2018) The affinity of the S9.6 antibody for double-stranded RNAs impacts the accurate mapping of R-loops in fission yeast. *J. Mol. Biol.*, **430**, 272–284.
53. Kinney,J.S., Viscidi,R.P., Vonderfecht,S.L., Eiden,J.J. and Yolken,R.H. (1989) Monoclonal antibody assay for detection of double-stranded RNA and application for detection of group A and non-group A rotaviruses. *J. Clin. Microbiol.*, **27**, 6–12.
54. Garcia-Muse,T. and Aguilera,A. (2016) Transcription-replication conflicts: how they occur and how they are resolved. *Nat. Rev. Mol. Cell Biol.*, **17**, 553–563.
55. Soderberg,O., Gullberg,M., Jarvius,M., Ridderstrale,K., Leuchowius,K.J., Jarvius,J., Wester,K., Hydbring,P., Bahram,F., Larsson,L.G., *et al.* (2006) Direct observation of individual endogenous protein complexes in situ by proximity ligation. *Nat. Methods*, **3**, 995–1000.
56. Makharashvili,N., Arora,S., Yin,Y., Fu,Q., Wen,X., Lee,J.H., Kao,C.H., Leung,J.W., Miller,K.M. and Paull,T.T. (2018) Sae2/CtIP prevents R-loop accumulation in eukaryotic cells. *eLife*, **7**, e42733.
57. Hatchi,E., Skourti-Stathaki,K., Ventz,S., Pinello,L., Yen,A., Kamieniarz-Gdula,K., Dimitrov,S., Pathania,S., McKinney,K.M., Eaton,M.L., *et al.* (2015) BRCA1 recruitment to transcriptional pause sites is required for R-loop-driven DNA damage repair. *Mol. Cell*, **57**, 636–647.
58. Skourti-Stathaki,K., Proudfoot,N.J. and Gromak,N. (2011) Human senataxin resolves RNA/DNA hybrids formed at transcriptional pause sites to promote Xrn2-dependent termination. *Mol. Cell*, **42**, 794–805.
59. Liang,Z., Liang,F., Teng,Y., Chen,X., Liu,J., Longerich,S., Rao,T., Green,A.M., Collins,N.B., Xiong,Y., *et al.* (2019) Binding of

FANCI-FANCD2 complex to RNA and R-loops stimulates robust FANCD2 monoubiquitination. *Cell Rep.*, **26**, 564–572.
60. Leuzzi,G., Taglialatela,A. and Ciccia,A. (2020) HATtracting nucleases to stalled forks. *Mol. Cell*, **80**, 177–180.
61. Li,Y., Li,Z., Dong,L., Tang,M., Zhang,P., Zhang,C., Cao,Z., Zhu,Q., Chen,Y., Wang,H., *et al.* (2018) Histone H1 acetylation at lysine 85 regulates chromatin condensation and genome stability upon DNA damage. *Nucleic Acids Res.*, **46**, 7716–7730.
62. Zhao,M., Geng,R., Guo,X., Yuan,R., Zhou,X., Zhong,Y., Huo,Y., Zhou,M., Shen,Q., Li,Y., *et al.* (2017) PCAF/GCN5-mediated acetylation of RPA1 promotes nucleotide excision repair. *Cell Rep.*, **20**, 1997–2009.
63. Clements,A., Rojas,J.R., Trievel,R.C., Wang,L., Berger,S.L. and Marmorstein,R. (1999) Crystal structure of the histone acetyltransferase domain of the human PCAF transcriptional regulator bound to coenzyme A. *EMBO J.*, **18**, 3521–3532.
64. Mimitou,E.P. and Symington,L.S. (2008) Sae2, Exo1 and Sgs1 collaborate in DNA double-strand break processing. *Nature*, **455**, 770–774.
65. Nicolette,M.L., Lee,K., Guo,Z., Rani,M., Chow,J.M., Lee,S.E. and Paull,T.T. (2010) Mre11-Rad50-Xrs2 and Sae2 promote 5' strand resection of DNA double-strand breaks. *Nat. Struct. Mol. Biol.*, **17**, 1478–1485.
66. Zhu,Z., Chung,W.H., Shim,E.Y., Lee,S.E. and Ira,G. (2008) Sgs1 helicase and two nucleases Dna2 and Exo1 resect DNA double-strand break ends. *Cell*, **134**, 981–994.
67. Tripathi,V., Agarwal,H., Priya,S., Batra,H., Modi,P., Pandey,M., Saha,D., Raghavan,S.C. and Sengupta,S. (2018) MRN complex-dependent recruitment of ubiquitylated BLM helicase to DSBs negatively regulates DNA repair pathways. *Nat. Commun.*, **9**, 1016.
68. Cheng,W.H., von Kobbe,C., Opresko,P.L., Arthur,L.M., Komatsu,K., Seidman,M.M., Carney,J.P. and Bohr,V.A. (2004) Linkage between Werner syndrome protein and the Mre11 complex via Nbs1. *J. Biol. Chem.*, **279**, 21169–21176.
69. Roques,C., Coulombe,Y., Delannoy,M., Vignard,J., Grossi,S., Brodeur,I., Rodrigue,A., Gautier,J., Stasiak,A.Z., Stasiak,A., *et al.* (2009) MRE11-RAD50-NBS1 is a critical regulator of FANCD2 stability and function during DNA double-strand break repair. *EMBO J.*, **28**, 2400–2413.
70. Schwab,R.A., Nieminuszczy,J., Shah,F., Langton,J., Lopez Martinez,D., Liang,C.C., Cohn,M.A., Gibbons,R.J., Deans,A.J. and Niedzwiedz,W. (2015) The Fanconi anemia pathway maintains genome stability by coordinating replication and transcription. *Mol. Cell*, **60**, 351–361.
71. Deans,A.J. and West,S.C. (2009) FANCM connects the genome instability disorders Bloom's Syndrome and Fanconi Anemia. *Mol. Cell*, **36**, 943–953.
72. Perego,M.G.L., Taiana,M., Bresolin,N., Comi,G.P. and Corti,S. (2019) R-loops in motor neuron diseases. *Mol. Neurobiol.*, **56**, 2579–2589.
73. Richard,P. and Manley,J.L. (2017) R Loops and links to human disease. *J. Mol. Biol.*, **429**, 3168–3180.
74. Halazonetis,T.D., Gorgoulis,V.G. and Bartek,J. (2008) An oncogene-induced DNA damage model for cancer development. *Science*, **319**, 1352–1355.
75. Young,K., Starling,N. and Cunningham,D. (2016) Targeting deficient DNA damage repair in gastric cancer. *Expert Opin. Pharmacother.*, **17**, 1757–1766.
76. Tadehara,M., Kato,T., Adachi,K., Tamaki,A., Kesen,Y., Sakurai,Y., Ichinoe,M., Koizumi,W. and Murakumo,Y. (2022) Clinicopathological significance of BRCAness in resectable pancreatic ductal adenocarcinoma and its association with anticancer drug sensitivity in pancreatic cancer cells. *Pancreas*, **51**, 183–189.
77. Lord,C.J. and Ashworth,A. (2016) BRCAness revisited. *Nat. Rev. Cancer*, **16**, 110–120.
78. Lai,E., Ziranu,P., Spanu,D., Dubois,M., Pretta,A., Tolu,S., Camera,S., Liscia,N., Mariani,S., Persano,M., *et al.* (2021) BRCA-mutant pancreatic ductal adenocarcinoma. *Br. J. Cancer*, **125**, 1321–1332.
79. Imai,S., Ooki,T., Murata-Kamiya,N., Komura,D., Tahmina,K., Wu,W., Takahashi-Kanemitsu,A., Knight,C.T., Kunita,A., Suzuki,N., *et al.* (2021) Helicobacter pylori CagA elicits BRCAness to induce genome instability that may underlie bacterial gastric carcinogenesis. *Cell Host Microbe*, **29**, 941–958.
80. Bhatia,V., Barroso,S.I., Garcia-Rubio,M.L., Tumini,E., Herrera-Moyano,E. and Aguilera,A. (2014) BRCA2 prevents R-loop accumulation and associates with TREX-2 mRNA export factor PCID2. *Nature*, **511**, 362–365.
81. Grunseich,C., Wang,I.X., Watts,J.A., Burdick,J.T., Guber,R.D., Zhu,Z., Bruzel,A., Lanman,T., Chen,K., Schindler,A.B., *et al.* (2018) Senataxin mutation reveals how R-loops promote transcription by blocking DNA methylation at gene promoters. *Mol. Cell*, **69**, 426–437.
82. Chen,Y.Z., Bennett,C.L., Huynh,H.M., Blair,I.P., Puls,I., Irobi,J., Dierick,I., Abel,A., Kennerson,M.L., Rabin,B.A., *et al.* (2004) DNA/RNA helicase gene mutations in a form of juvenile amyotrophic lateral sclerosis (ALS4). *Am. J. Hum. Genet.*, **74**, 1128–1135.
83. Moreira,M.C., Klur,S., Watanabe,M., Nemeth,A.H., Le Ber,I., Moniz,J.C., Tranchant,C., Aubourg,P., Tazir,M., Schols,L., *et al.* (2004) Senataxin, the ortholog of a yeast RNA helicase, is mutant in ataxia-ocular apraxia 2. *Nat. Genet.*, **36**, 225–227.
84. Brustel,J., Kozik,Z., Gromak,N., Savic,V. and Sweet,S.M.M. (2018) Large XPF-dependent deletions following misrepair of a DNA double strand break are prevented by the RNA:DNA helicase Senataxin. *Sci. Rep.*, **8**, 3850.
85. Tubbs,A. and Nussenzweig,A. (2017) Endogenous DNA damage as a source of genomic instability in cancer. *Cell*, **168**, 644–656.
86. Lee,S.Y., Miller,K.M. and Kim,J.J. (2023) Clinical and mechanistic implications of R-loops in human leukemias. *Int. J. Mol. Sci.*, **24**, 5966.
87. Chiang,H.C., Qi,L., Mitra,P., Hu,Y. and Li,R. (2024) R-loop functions in Brca1-associated mammary tumorigenesis. bioRxiv doi: ttps://doi.org/10.1101/2024.02.14.580374, 16 February 2024, preprint: not peer reviewed.
88. Chiang,H.C., Zhang,X., Li,J., Zhao,X., Chen,J., Wang,H.T., Jatoi,I., Brenner,A., Hu,Y. and Li,R. (2019) BRCA1-associated R-loop affects transcription and differentiation in breast luminal epithelial cells. *Nucleic. Acids. Res.*, **47**, 5086–5099.
89. Racca,C., Britton,S., Hedouin,S., Francastel,C., Calsou,P. and Larminat,F. (2021) BRCA1 prevents R-loop-associated centromeric instability. *Cell Death. Dis.*, **12**, 896.
90. Wang,Y., Ma,B., Liu,X., Gao,G., Che,Z., Fan,M., Meng,S., Zhao,X., Sugimura,R., Cao,H., *et al.* (2022) ZFP281-BRCA2 prevents R-loop accumulation during DNA replication. *Nat. Commun.*, **13**, 3493.
91. Cristini,A., Ricci,G., Britton,S., Salimbeni,S., Huang,S.N., Marinello,J., Calsou,P., Pommier,Y., Favre,G., Capranico,G., *et al.* (2019) Dual processing of R-loops and topoisomerase I induces transcription-dependent DNA double-strand breaks. *Cell Rep.*, **28**, 3167–3181.

Received: March 5, 2024. **Revised:** June 4, 2024. **Editorial Decision:** June 12, 2024. **Accepted:** June 19, 2024